

## 14. SITE 726<sup>1</sup>

### Shipboard Scientific Party<sup>2</sup>

#### HOLE 726A

**Date occupied:** 23 September 1987

**Date departed:** 24 September 1987

**Time on hole:** 20 hr, 15 min

**Position:** 17°48.965'N, 57°22.290'E

**Water depth (sea level; corrected m, echo-sounding):** 330.8

**Water depth (rig floor; corrected m, echo-sounding):** 341.3

**Bottom felt (m, drill pipe):** 340.1

**Penetration (m):** 186.3

**Number of cores:** 22

**Total length of cored section (m):** 186.3

**Total core recovered (m):** 110.1

**Core recovery (%):** 59.1

#### **Oldest sediment cored**

Depth sub-bottom (m): 186.3

Nature: limestone

Age: Eocene (?)

Measured velocity (km/s): 5.89–6.13

**Principal results:** Site 726 is located on what was assumed to be a pre-Neogene basement high that coincides with the shelf break. This shelf is landward of a slope basin filled with thick (up to 2 km) Neogene sediment on the Oman continental margin. The main objective at Site 726 was to identify the nature and age of rocks that underlie Neogene hemipelagic sediments in much of the Leg 117 study area. Of note are the following findings:

1. Repeated alternations from anoxic to oxic conditions in the bottom water resulted in alterations of bioturbated lag deposits with laminated organic-rich layers in the hemipelagic Miocene to Holocene sediment.

2. The preservation of biogenic opal in upper Pliocene sediments parallels opal occurrences at other sites on the margin.

3. Shallow-water nummulitic limestones are dolomitized and are similar to limestones overlying ophiolitic basement on Masirah Island in age and facies. Cementation of the limestone occurred in distinct phases and may be partly related to vadose, fresh-water aquifers.

4. Erosion of shallow-water limestones or nondeposition at the site occurred during much of the Paleogene and lower Miocene.

The recovered section at Site 726 shows the influence that local tectonism and position of the site to the upper boundary of the oxygen-minimum zone have on sediment facies. Hemipelagic sediments of the Neogene reflect repeated oscillations between anoxia and oxic in bottom waters since the late Miocene. Over much of the Oman continental margin, basement appears to be overlain by shallow-water carbonate sediments, which have been uplifted and cemented by vadose cements.

#### BACKGROUND AND OBJECTIVES

Site 726 is located in a water depth of about 330 m at 17°48.965'N, 57°22.290'E on the continental margin of Oman. Much of the Oman margin is characterized by a narrow shelf bordered by an extremely steep continental slope, which is thought to be a megashear associated with formation of the margin (Whitmarsh, 1979; Stein and Cochran, 1985). However, the margin between Ras Sharbithat and Ras al Madrasah has a relatively wide continental shelf (about 50 miles) and a series of linear sedimentary basins along the upper continental slope (Fig. 1). This area of the slope and margin may be partly composed of the upthrust ophiolite complex that is observed on the island of Masirah north of Site 726 (Moseley and Abbotts, 1979).

The location of Site 726 is shown in Figure 2, and its structural and depositional setting is shown in Figure 3. Site 726 is located about 5 km landward of the eastern edge of a faulted block that is thought to be an ophiolite complex (Fig. 3B). This block forms the western boundary of the slope basin. The seismic reflection profiles (Figs. 3A, 3B) show gently eastward-dipping reflective layers from about 0.12 to 0.22 s that are truncated to the east and are draped like a conformable pelagic (?) cap. The strong reflector at 0.22 s (Figs. 3A, 3B) is underlain by more diffuse reflections that are thought to be the ophiolitic basement. However, deep structure is observed near the eastern fault (Fig. 3B). In general, this location reveals older, conformable reflectors having an unknown relationship to basement and that are truncated and draped by pelagic sediments. Because of the shallow water depth of Site 726, sediments were expected to be more sandy and possibly winnowed, compared with sediments of slope basins.

Specific objectives for drilling at Site 726 were:

1. To obtain samples of the basement complex and its overlying sediments to help constrain the tectonic and depositional history of the margin and the slope basins.

2. To provide an additional shallow-water end-member for a depth transect of sediments that will be used to examine the organic-rich sedimentary facies of the margin and to establish their relationship to the oxygen-minimum zone and its spatial variation through time.

#### OPERATIONS

*JOIDES Resolution* departed Site 725 at 2400 hr on 22 September 1987 and relocated to Site 726 for a seismic survey and drilling operations. We established a seismic dip line and confirmed the RC2704 strike line during good global positioning satellite (GPS) coverage, retrieved seismic gear, and lowered the taut-wire beacon in a water depth of 331 m at 1000 hr on 23 September. The final position of Site 726 was established as 17°48.965'N, 57°22.290'E (Fig. 4).

Core 117-726A-1H was shot at 1200 hr, followed by a rapid succession of five advanced piston corer (APC) cores (0–54.1 meters below seafloor [mbsf]) and a deployment of the *in-situ* pore-water sampler after Core 117-726A-4H. An overpull of

<sup>1</sup> Prell, W. D., Niituma, N., et al., 1989. *Proc. ODP, Init. Repts.*, 117: College Station, TX (Ocean Drilling Program).

<sup>2</sup> Shipboard Scientific Party is as given in list of Participants preceding the contents.

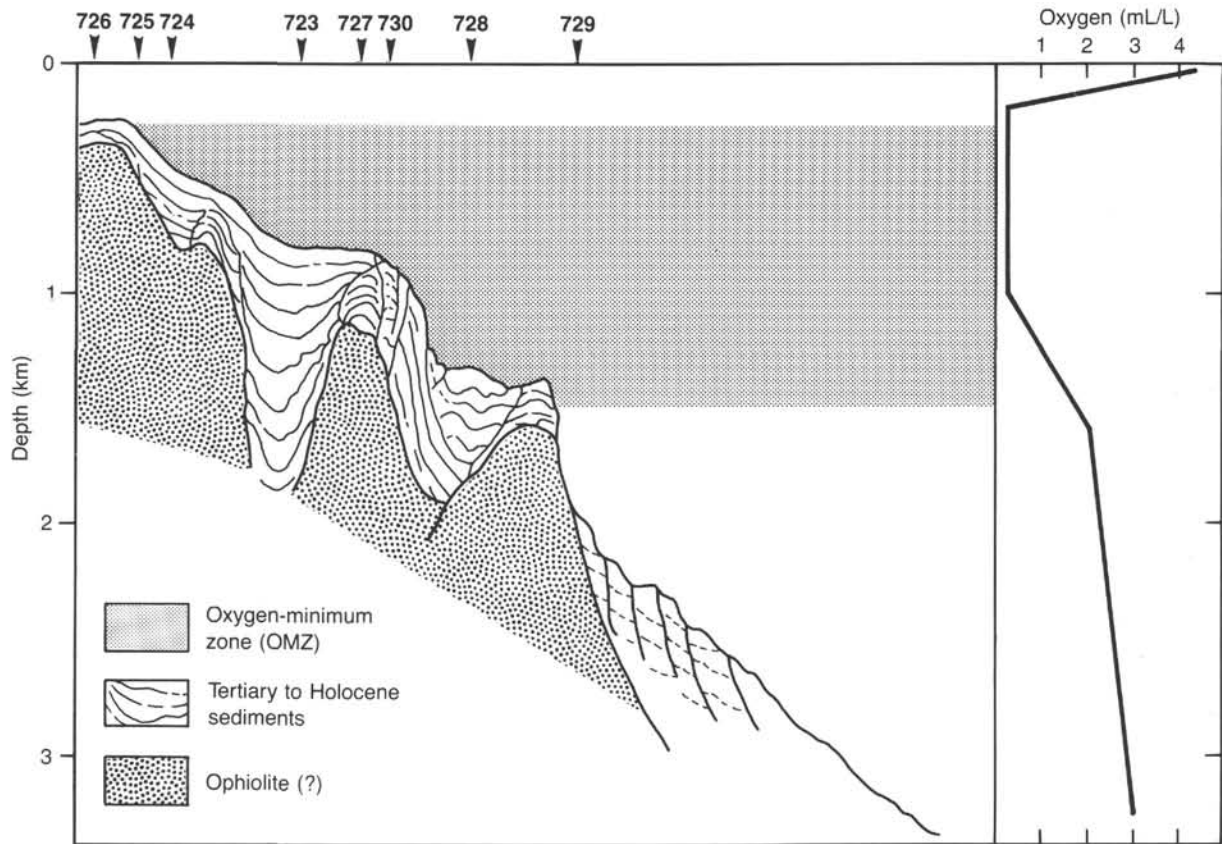


Figure 1. Structure of the Oman margin and the oxygen-minimum zone: the schematic seismic-reflection profile shows a series of basement ophiolite blocks and the sedimentary basins between them. The concentration of oxygen in the water column (RC2704, unpubl. data) defines the depth range of the oxygen-minimum zone and where it impinges on the margin. Schematic location of Site 726 is indicated.

80,000 lb when retrieving Core 117-726A-6H made coring in extended-core-barrel (XCB) mode necessary, starting with Core 117-726A-7X. Recovery in the section cored by the APC was 103%. By 0120 hr, 24 September, Core 117-726A-22X had been retrieved from a total depth of 186.3 mbsf. Core 117-726A-22X was stuck in the bit and the bottom-hole assembly (BHA) had to be pulled out to recover the core barrel on the rig floor. In the cemented dolomite that composed the section below Core 117-726A-16X, penetration and recovery decreased (recovery in the interval cored by the XCB was 40.7% and generally below 10% in the limestone/dolomite), and the hoped-for penetration into ophiolitic basement seemed unattainable within the allocated time (Table 1). Thus, we terminated Hole 726A, displaced it with mud, and pulled the drill string. We were under way to Site 727 by 0830 hr on 24 September.

## LITHOSTRATIGRAPHY

### Introduction

The sediments and rocks recovered at Site 726 are divided into two lithologic units (Fig. 5). Unit I is composed of two subunits, which are composed of (1) silty clays of Pleistocene and Holocene age and (2) an alternation between organic-carbon-rich silty clays and foraminifer-rich clayey silts of Pleistocene to late Miocene age. Unit II is composed of Eocene (?) shallow-water limestones and dolomites.

### Unit I (Depth: 0–131.1 mbsf; Age: Holocene to late Miocene)

Core 117-726-1H to Section 117-726A-14X, CC.

Lithologic Unit I is divided into two subunits that consist of bioturbated calcareous silty clays and alternations of organic-carbon-rich silty clays and foraminifer-rich silts.

#### Subunit IA (Depth: 0–32.05 mbsf)

Subunit IA consists of calcareous silty clays to marly calcareous ooze with increasing foraminifer content upsection. The color varies from olive (5Y 4/3 to 4/4) to dark olive gray (5Y 3/2). The sediment is composed of 10% to 30% foraminifers, 5% to 40% nannofossils, 10% to 40% detrital calcite, 30% clay, 5% to 15% quartz, and 0% to 2% dolomite (Fig. 6). Small shell fragments are abundant, while soft and hard phosphorite concretions are rare. Bioturbation is not clearly visible in the first two cores due to slight drilling disturbance and lack of differences in lithology. However, mottling occurs in Cores 117-726A-3H and 117-726A-4H. Organic carbon values range from 0.4% to 1.1%, while the carbonate content varies from 53% to 63% (Fig. 7 and Table 2).

#### Subunit IB (Depth: 32.05–131.1 mbsf)

Subunit IB consists of a suite of laminated, organic-rich, silty clays to marly nannofossil ooze to chalk, interspersed with foraminifer-rich muds. The subunit is Pleistocene to late Miocene in age. The coarse-grained, foraminifer-rich muds are

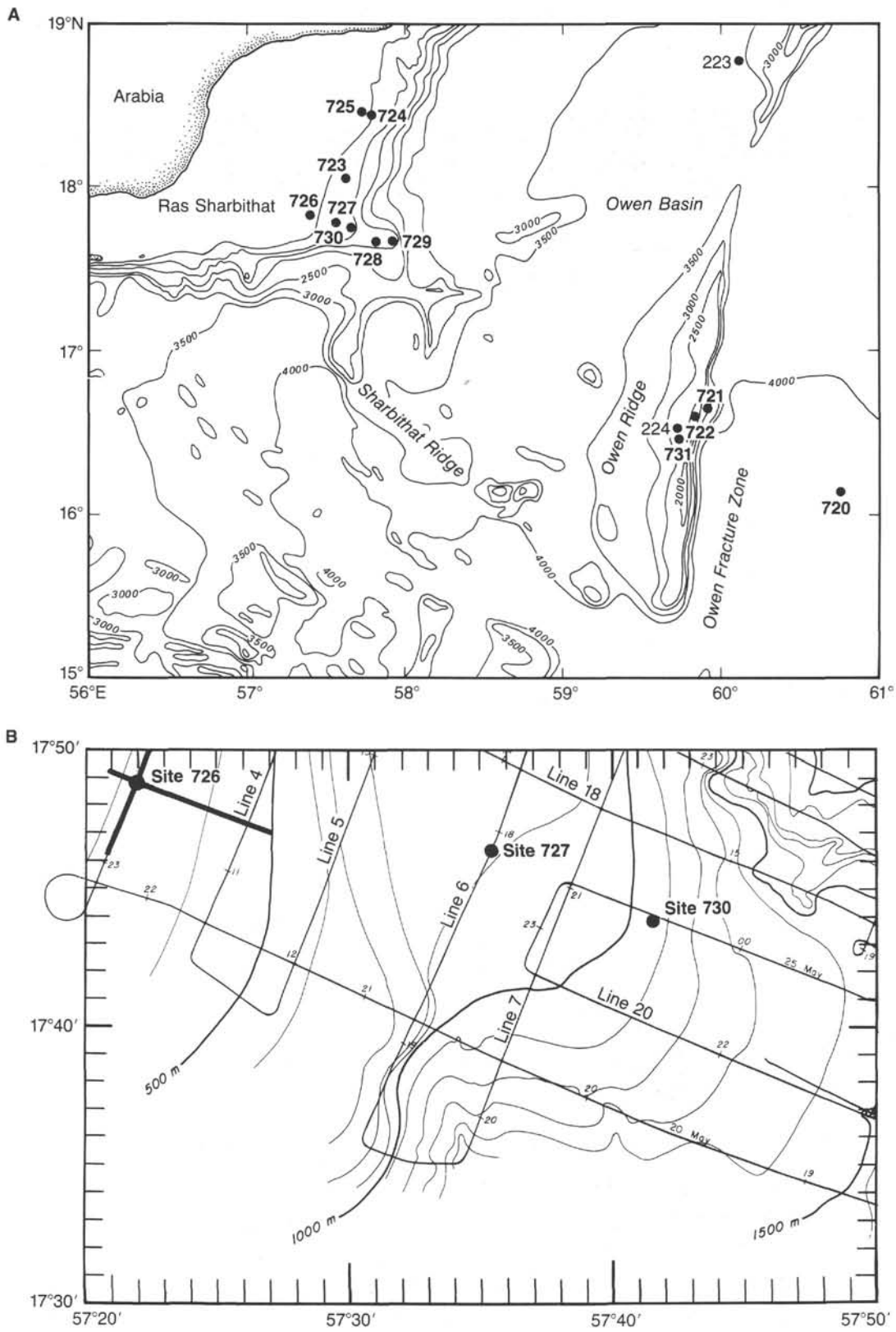


Figure 2. **A.** Bathymetry of the Oman margin and the location of Site 726. **B.** Detailed location of Site 726 and seismic profiles shown in Figure 3. Bathymetry data from the site survey (RC2704, 1986).

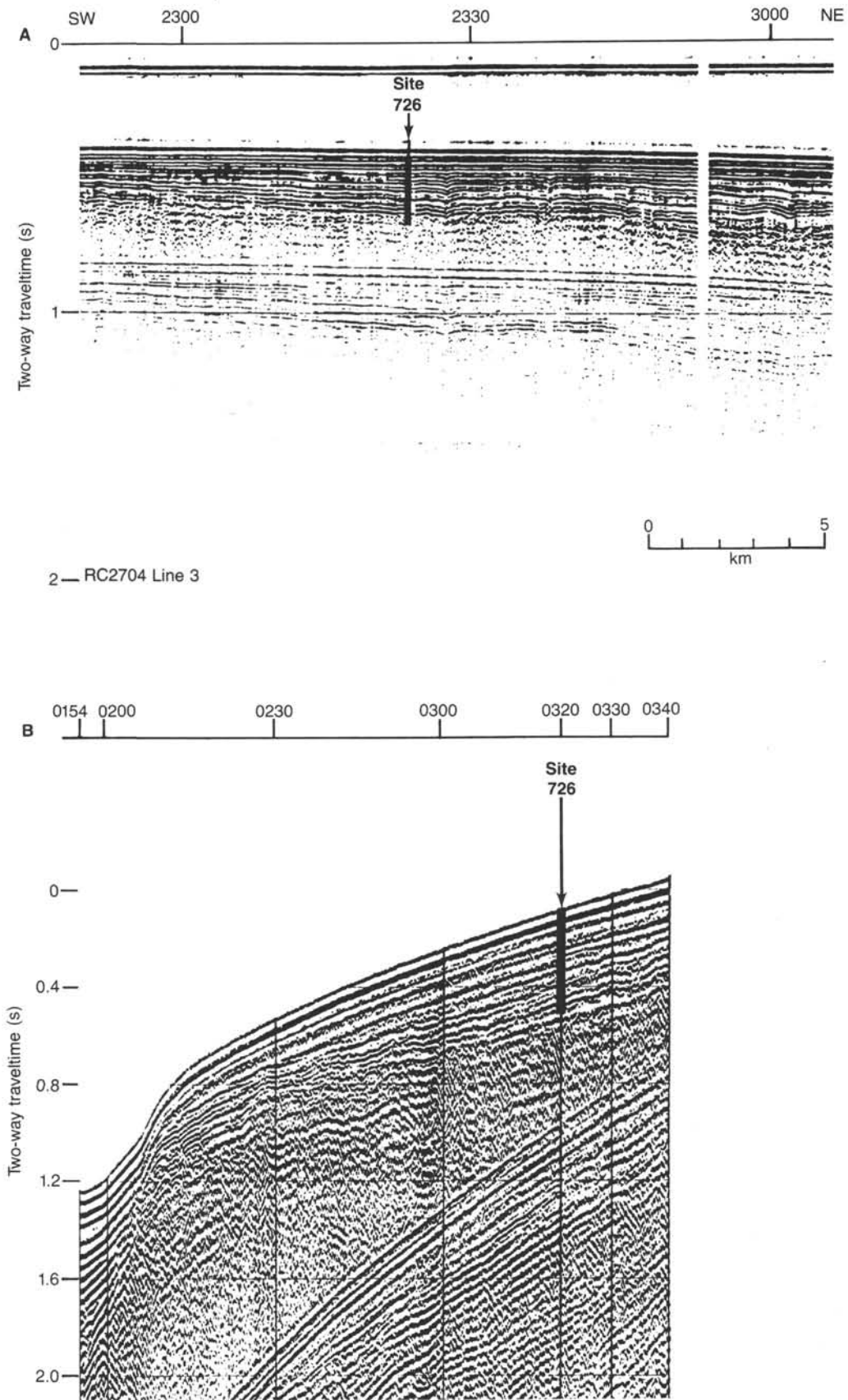


Figure 3. **A.** Single-channel seismic-reflection profiles showing the structural and depositional setting of Site 726. RC2704 Line 3 is along the strike of the basement block and shows the continuity of the basement (?) reflector. **B.** Line 5, *JOIDES Resolution*, is perpendicular to the trend of the faulted basin and shows bounding basement blocks and truncated sediments.

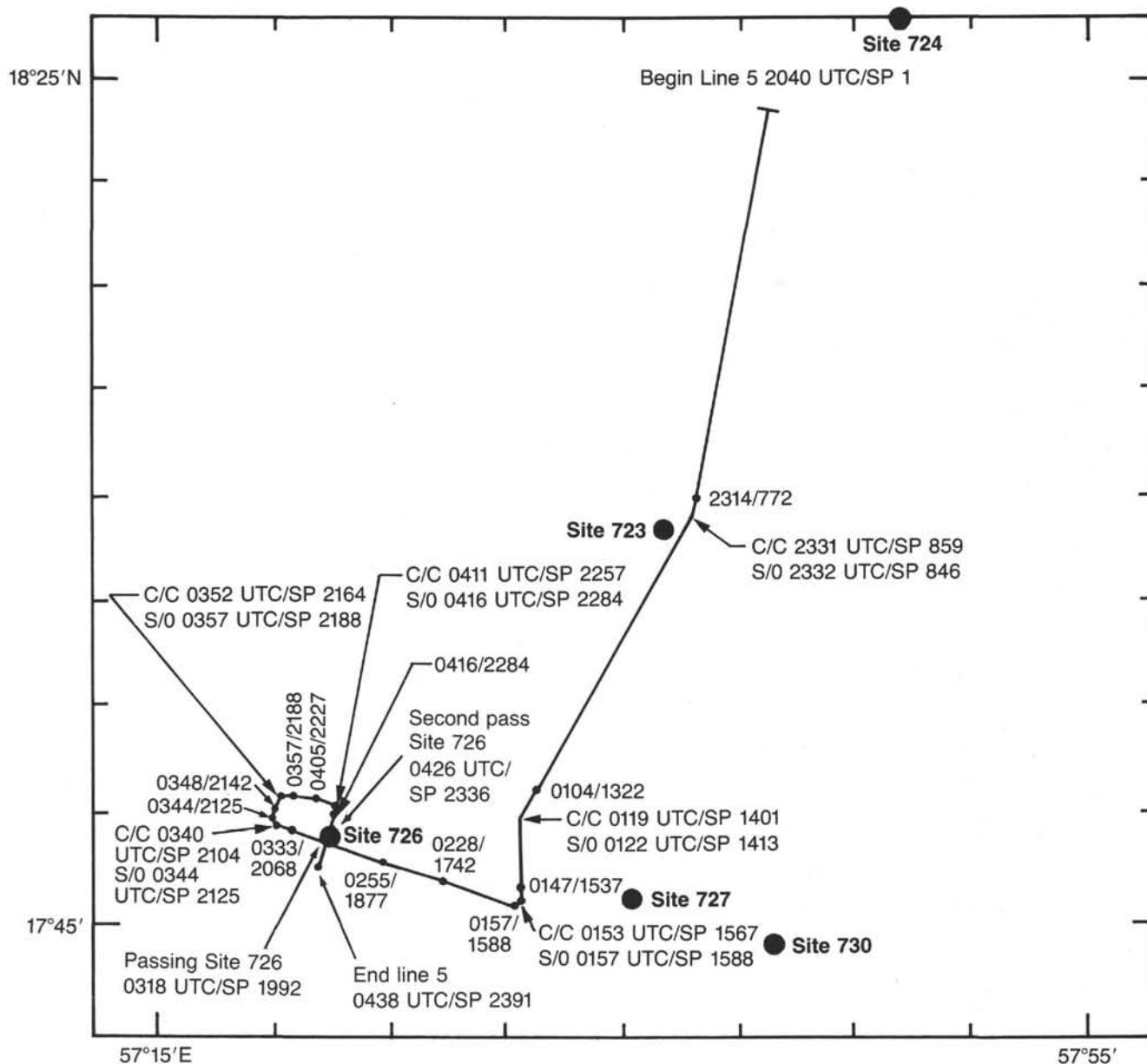


Figure 4. Ship's track line during relocation from Site 725 and seismic survey of Site 726.

thought to represent lag deposits, as explained below. Colors range from olive (5Y 4/3 to 4/4) to dark olive gray (5Y3/2) to very dark gray (5Y 3/1) for the silty clays and marly oozes, and from olive (5Y 4/3 to 4/4) to olive gray (5Y 4/2) for the foraminifer-rich layers. Subunit IB displays little to no bioturbation, and laminations are preserved in 1- to 2-m-thick beds in Cores 117-726A-5H to 117-726A-9X (41.3–77.5 mbsf). This interval has a higher clay content (35% to 65%) and a higher content of organic carbon (3% to 4.8%) than the other parts of Subunit IB. The discrete laminated beds are composed of individual laminae 1 to 5 cm thick. Only in Core 117-726A-9X do the laminae contain relatively high amounts of diatoms (up to 25%, 76.2–77.5 mbsf, Fig. 6). Black phosphatic concretions having a diameter of 0.5 to 1.5 cm occur throughout Subunit IB (Fig. 8).

The nonlaminated part of Subunit IB consists of locally dolomitic, foraminifer-bearing marly nannofossil ooze to mud, with an average inorganic calcite content of 15% (Fig. 6). A coarse-grained part of the nonlaminated portion is developed as

lag deposits, which are composed of foraminifer-rich muds and nannofossil-foraminifer oozes and which are interbedded with the more organic-rich lithologies of Subunit IB. These are found in two intervals, from Cores 117-726A-4H to 117-726A-6H (32.2–50.9 mbsf) and from Cores 117-726A-8X to 117-726A-14X (65.1–131.1 mbsf). Thus, they overlap with the upper and the lower portions of the laminated zone (Fig. 5). The lag layers are slightly to inversely graded, 3 to 30 cm thick, and have their maximum grain size at the base or in the middle of the beds (Figs. 9 through 11). These layers often show bioturbation mottling with distinctive infill patterns of foraminifer-rich muds into the underlying, nonbioturbated to sparsely bioturbated facies of Subunit IB (Figs. 9 and 10). In the interval from Cores 117-726A-11X to 117-726A-14X (92.4–131.1 mbsf), they form composite lag beds, which become more abundant downhole. Compositionally, lag deposits concentrate phosphoric concretions having a diameter of 1 mm to 0.5 cm, fish bones and fish teeth, and many foraminifer tests with phosphatic incrustations. Be-

Table 1. Coring summary for Site 726.

Core no.	Date (Sept. 1987)	Time (UTC)	Depth (mbsf)	Cored (m)	Recovered (m)	Recovery (%)
117-726A-						
1H	23	1230	0-6.9	6.9	6.90	100.0
2H	23	1250	6.9-16.3	9.4	9.92	105.0
3H	23	1310	16.3-25.8	9.5	9.93	104.0
4H	23	1325	25.8-35.3	9.5	9.61	101.0
5H	23	1430	35.3-44.7	9.4	9.93	105.0
6H	23	1455	44.7-54.1	9.4	0.05	106.0
7X	23	1535	54.1-63.6	9.5	7.91	83.2
8X	23	1550	63.6-73.2	9.6	9.44	98.3
9X	23	1605	73.2-82.8	9.6	5.22	54.4
10X	23	1620	82.8-92.4	9.6	7.23	75.3
11X	23	1635	92.4-102.1	9.7	7.04	72.6
12X	23	1645	102.1-111.8	9.7	0.24	2.5
13X	23	1700	111.8-121.4	9.6	8.67	90.3
14X	23	1730	121.4-131.1	9.7	2.72	28.0
15X	23	1800	131.1-140.7	9.6	1.09	11.3
16X	23	1850	140.7-148.1	7.4	0.59	8.0
17X	23	1950	148.1-154.1	6.0	0.35	5.8
18X	23	2045	154.1-164.1	10.0	0.20	2.0
19X	23	2150	164.1-173.7	9.6	1.79	18.6
20X	23	2330	173.7-183.4	9.7	1.08	11.1
21X	24	0120	183.4-183.8	0.4	0.12	30.0
22X	24	0830	183.8-186.3	2.5	0.18	7.2

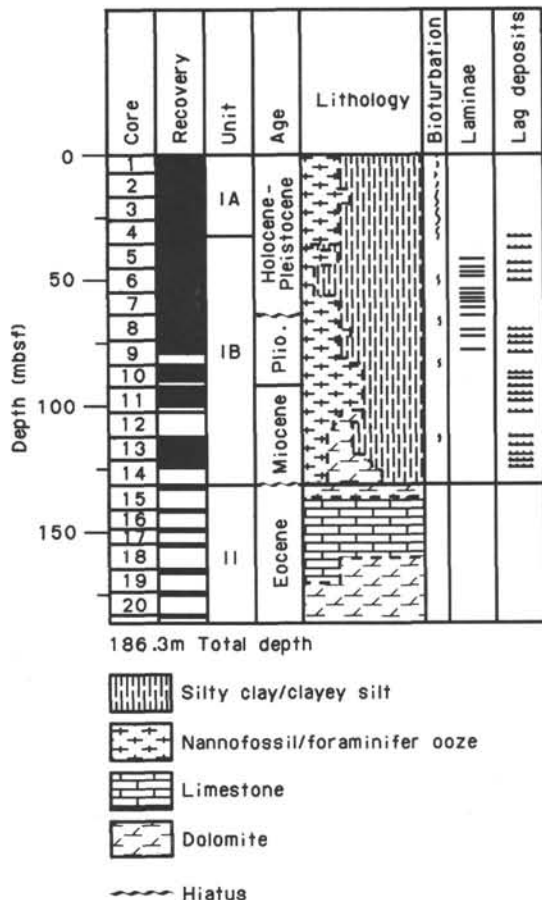


Figure 5. Lithostratigraphy of Site 726.

low Core 117-726A-11X, the lag layers are more and more affected by dolomitization (Fig. 5).

**Unit II (Depth: 131.1-186.3 mbsf; Age: Eocene [?])**

Core 117-726-15X to Section 117-726A-22X, CC.

Lithologic Unit II is composed of a partly dolomitized shallow-water limestone with carbonate contents higher than 95%. Although recovery was low throughout lithologic Unit II, two primary and one diagenetic facies types were distinguished. The former includes a large foraminifer- and algae-dominated facies with primary components, while the latter is a dolomitized facies. The foraminifer facies is characteristic of the top of the carbonate complex and is progressively replaced by the algae-dominated facies toward the base of the recovered section. The dolomite facies occurs in a zone at the transition from Unit I to Unit II and in the last four cores of the carbonate sequence. Cementation and dolomitization generally increase downhole.

**Facies IIA (Foraminifer-Bearing Wackestone to Packstone)**

Facies IIA (Fig. 12) is a white, indistinctly bedded, foraminifer-bearing wackestone to packstone containing centimeter-sized specimens of *Nummulites cf. planulatus* and *Actinocyclus* (see "Biostratigraphy" section, this chapter). The matrix of this weakly lithified rock is micritic, with cementation concentrated at the grain contacts in the form of a meniscuslike cement, which is a possible indicator of cementation in the vadose zone (e.g., Bathurst, 1975). The interparticle porosity in the foraminifer-bearing wackestone is high (see "Physical Properties" section, this chapter).

**Facies IIB (Algae-Dominated Wackestone)**

Facies IIB displays 1- to 4-cm-thick, irregularly shaped, calcitic spheres of oncolithic algae (Figs. 13 and 14) and 1-cm-thick branches of coralline algae (Fig. 15). A portion of the coralline algae is concentrated in beds up to 5 cm thick and was observed in nongrowth positions. Both characteristics indicate reworking and transport of the bioclasts by currents.

**Facies IIC (Biomoldic Dolomite)**

Dolomitized equivalents of Facies IIA and IIB are found at the top and the base of the recovered carbonate sequence. The dolomites are light gray (2.5Y 7/2) to gray (2.5Y 6/0), contain silt-sized rhombs, and show abundant biomoldic casts of the foraminifer and other fossils found in Facies IIA and IIB. Ex-

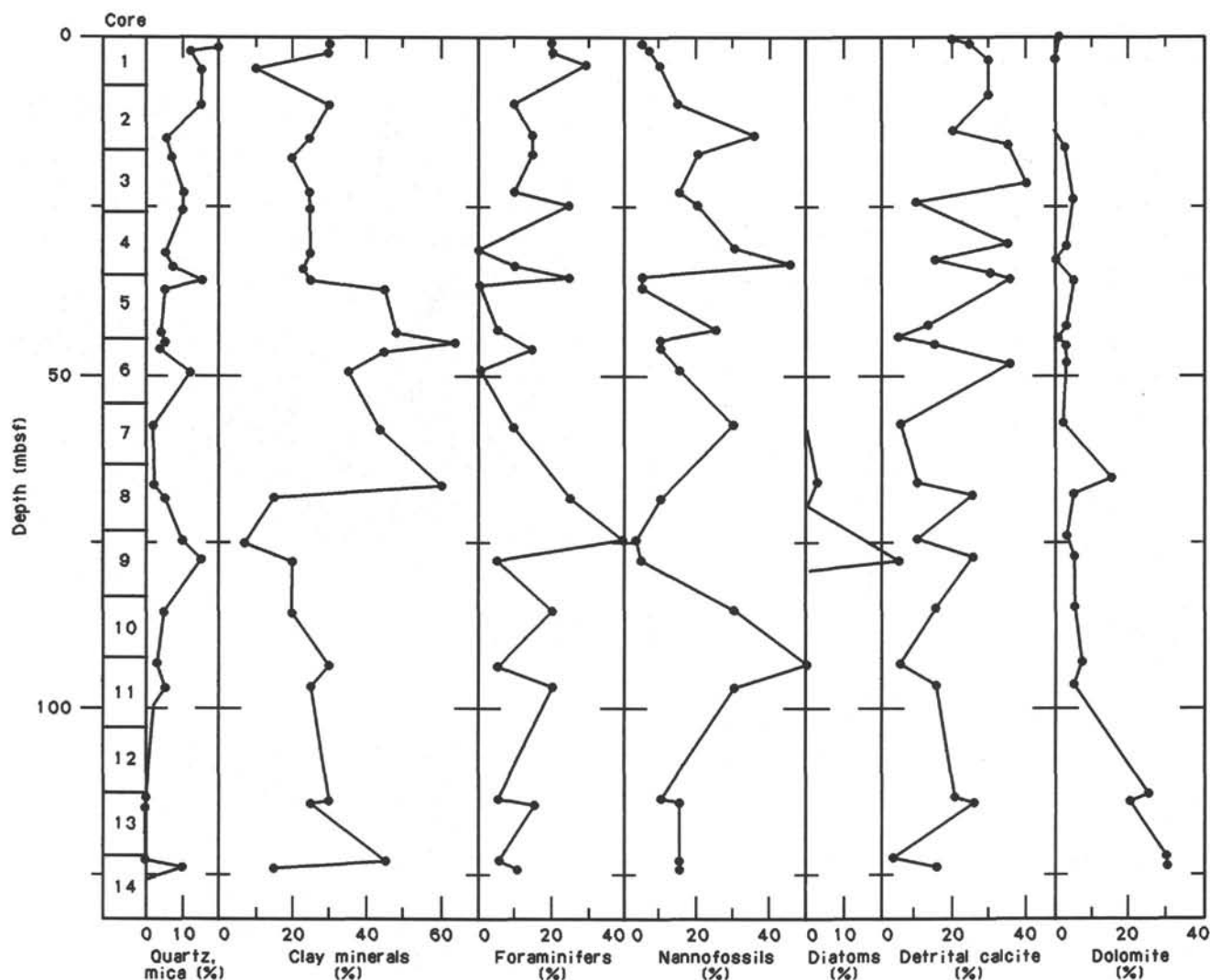


Figure 6. Smear-slide composition (in areal percentage) of lithologic Unit I.

cept for an occurrence at the contact with lithologic Unit I, dolomitization increases downhole. Based on thin sections from rocks in Cores 117-726A-16X to 117-726A-22X, the following preliminary stages of progressive diagenesis can be established:

1. Meniscuslike, micritic calcite cements the contacts of larger grains, while micritic calcite cementation affects the rock matrix (Core 117-726A-16X, 141 mbsf; Figs. 12 and 13).
2. Dolomitization of the rock matrix destroys most of its fabric, while larger fossils are not affected and remain calcitic (e.g., Core 117-726A-19X, 164 mbsf; Fig. 15).
3. Dissolution of calcitic allochems, such as large foraminifers, algae, etc., creates a biomoldic porosity (Fig. 16). On the surface of these molds, drusy dolomite crystals may grow to form a dolomitic spar in a relatively late stage of diagenesis. Locally, a final calcite spar follows the dolomitic spar.

The general downhole increase in diagenesis and lithification within lithologic Unit II results in a decrease in porosity downhole. Porosity decreases from about 40% in the upper part of Unit II to nearly zero in the lower part (see "Physical Properties" section, this chapter).

## Discussion

### Unit II

The foraminifer and algae facies indicate a warm, shallow-water environment. Diagenetic fabrics in the carbonate and lower dolomite complex document increasing lithification with depth, which begins with a grain-contact cementation in the upper part and proceeds to dolomitization in the lower portion of the sequence at Site 726. This pattern could be interpreted as a "frozen" diagenetic zonation, which still displays the diagenetic pattern achieved during or immediately after deposition of the upper part of Unit II. For instance, a diagenetic zonation similar to that described here is expected from several diagenetic models, including a groundwater-seawater mixing zone established after tectonic uplift. However, the question remains as to why these limestones were not fully cemented later. The unconformity between lithologic Units I and II could indicate a long phase of uplift and erosion, and contact with meteoric pore waters would cement the limestone within a short period of time. Without a better understanding of the local tectonic history, however, we cannot hope to answer this question.

Dolomitic zones found above, and especially below, the unconformity, as well as the relatively early onset of lithification

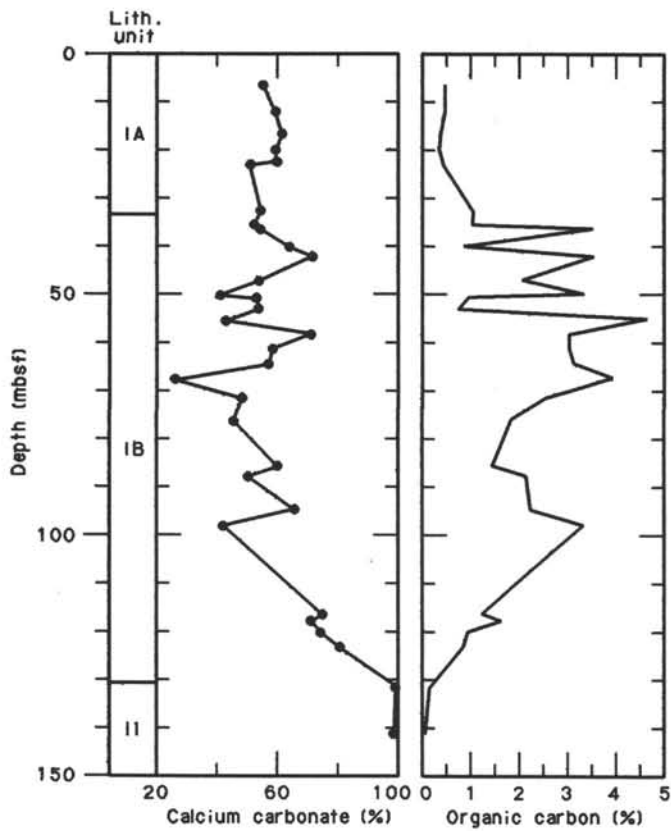


Figure 7. Carbonate and organic carbon contents at Site 726.

Table 2. Carbonate and organic carbon data from Site 726.

Core, section, interval (cm)	Depth (mbsf)	Total carbon (%)	Inorganic carbon (%)	Organic carbon (%)	CaCO <sub>3</sub> (%)
117-726A-					
1H-5, 52-54	6.52	7.32	6.78	0.54	56.5
2H-4, 60-62	12.00	7.84	7.30	0.54	60.8
2H-7, 60-62	16.50	7.99	7.56	0.43	63.0
3H-3, 50-52	19.80	7.75	7.29	0.46	60.7
3H-4, 145-150	22.25	7.88	7.32	0.56	61.0
3H-5, 50-52	22.80	6.82	6.30	0.52	52.5
4H-5, 50-52	32.30	7.83	6.73	1.10	56.1
4H-7, 30-32	35.10	7.60	6.46	1.14	53.8
5H-1, 80-82	36.10	10.38	6.72	3.66	56.0
5H-3, 130-132	39.60	8.80	7.88	0.92	65.6
5H-5, 52-54	41.82	12.50	8.81	3.69	73.4
6H-2, 50-52	46.70	8.78	6.68	2.10	55.6
6H-4, 50-52	49.70	8.49	5.09	3.40	42.4
6H-4, 119-120	50.39	7.63	6.59	1.04	54.9
6H-6, 50-52	52.70	7.50	6.65	0.85	55.4
7X-1, 98-100	55.08	10.11	5.32	4.79	44.3
7X-3, 100-102	58.10	11.85	8.72	3.13	72.6
7X-5, 100-102	61.10	10.40	7.21	3.19	60.1
8X-1, 52-54	64.12	10.30	7.03	3.27	58.6
8X-3, 52-54	67.12	7.33	3.25	4.08	27.1
8X-6, 27-29	71.37	8.67	6.05	2.62	50.4
9X-2, 117-119	75.87	7.69	5.75	1.94	47.9
9X-2, 119-120	75.89	7.51	5.60	1.91	46.7
10X-2, 127-129	85.57	9.03	7.45	1.58	62.1
10X-4, 31-33	87.61	8.56	6.27	2.29	52.2
11X-2, 60-62	94.50	10.44	8.09	2.35	67.4
11X-4, 100-102	97.90	8.65	5.20	3.45	43.3
13X-3, 130-132	116.10	10.54	9.24	1.30	77.0
13X-4, 119-120	117.49	10.43	8.73	1.70	72.7
13X-6, 66-68	119.96	10.23	9.18	1.05	76.5
14X-2, 5-7	122.95	10.86	9.93	0.93	82.7
15X-1, 58-60	131.68	12.41	12.17	0.24	101.4
16X, CC 22-24	141.13	12.26	12.07	0.19	100.5

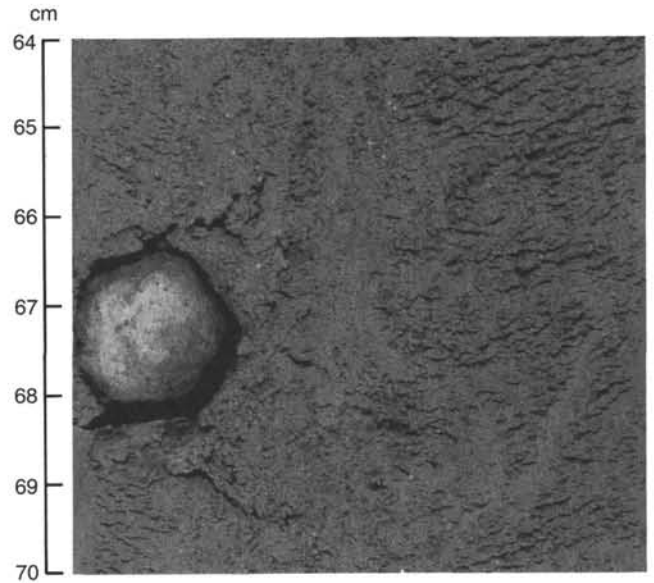


Figure 8. Large phosphorite concretions (1.5 cm), Subunit IB (Section 117-726A-6H-6, 64-70 cm).

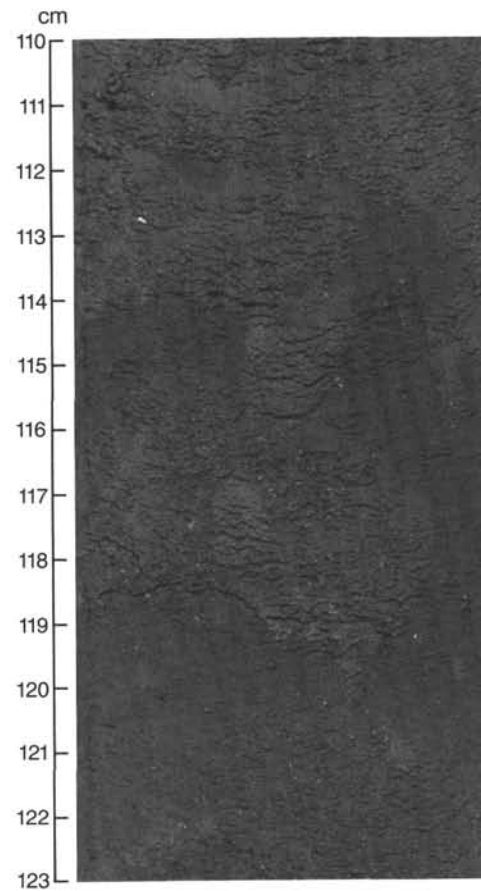


Figure 9. Bioturbated infill of foraminifer mud from an overlying lag deposit into sparsely to unbioturbated silty clay; Subunit B (Section 117-736A-5H-6, 110-123 cm).

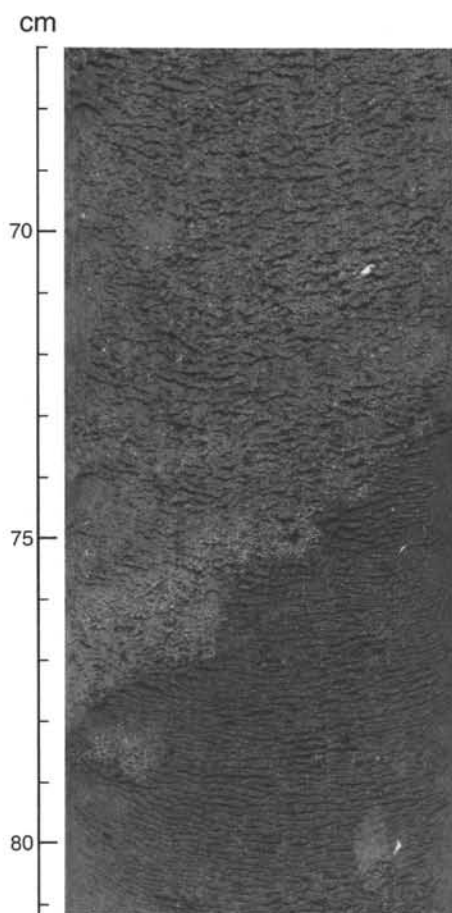


Figure 10. Foraminifer-rich lag deposit that exhibits a relatively coarse-grained, sharp base and that shows bioturbated infill into the underlying, sparsely bioturbated silty clay; Subunit IB (Section 117-726A-5H-1, 67–82 cm).

(110 m in chalky layers of Unit I), may result from diagenetic effects of both the lateral movements of pore water in the porous carbonates and the high heat-flow values. Pore waters from lithologic Unit I show increasing chlorinity and sulfate values downhole, and a decreasing magnesium/calcium ratio (see “Inorganic Geochemistry” section, this chapter). In addition, heat-flow measurement gives a value that is three times higher than that at the other sites drilled at the Oman margin (see “*In-Situ* Pore-Water Sampling and Downhole Temperature and Heat-Flow Measurements” chapter, this volume).

The recovered Paleogene carbonates may correlate with similar, but more lithified, shallow-water limestones and dolomites found in Oman (Powers et al., 1966) and on the island of Masirah (Moseley and Abbotts, 1979). The uplift of the carbonate sequence at Site 726 occurred sometime between the Eocene and the late Miocene, as documented by the unconformity. It may be related to compressional movements along dextral, northeast-striking, strike-slip faults that took up differential movements between the Indian and the African-Arabian plates (Moseley and Abbotts, 1979; Whitmarsh, 1979).

#### Unit I

Three observations regarding the sediments of lithologic Unit I at Site 726 are briefly discussed as follows:

1. The increase of lag deposits downhole documents a high degree of reworking in the upper Miocene section. Reworking

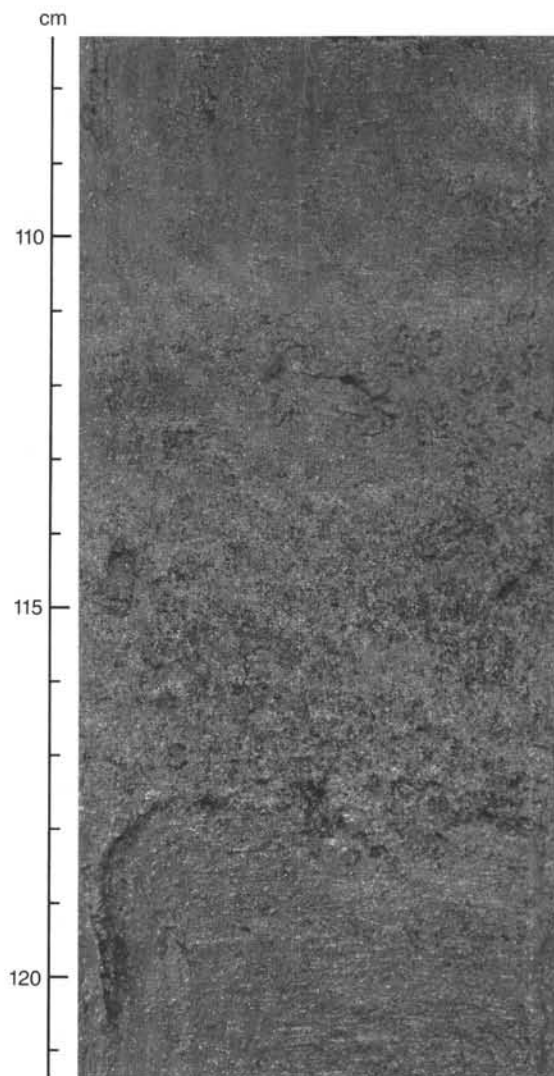


Figure 11. Lag deposit composed of foraminifer-rich mud having an inversely graded base; Subunit IB (Section 117-726A-13X-3, 107–121 cm).

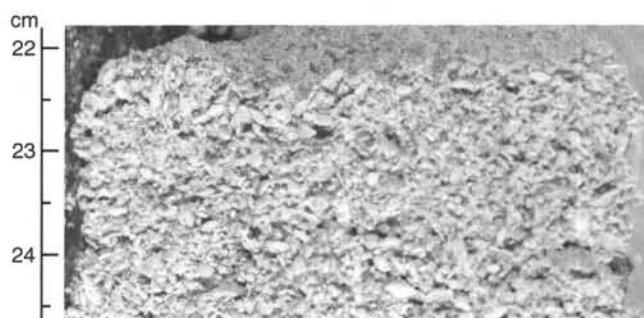


Figure 12. Nummulitic wackestone to packstone that exhibits grain contact cementation and high interparticle porosity; Unit II (Section 117-726A-16X, CC, 2–25 cm, Facies IIA).

may indicate that Site 726 had a somewhat shallower water depth in the late Miocene than it does today. This may be explained by a combination of the effects of subsidence, sedimentation, and sea-level variation (Haq et al., 1987).

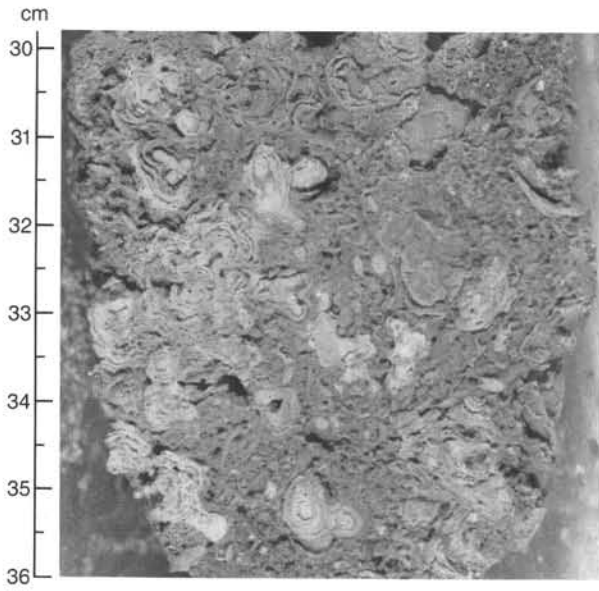


Figure 13. Incompletely cemented, highly porous, oncolithic limestone with cementation occurring at the grain contacts; Unit II (Section 117-726A-16X, CC, 30-36 cm, Facies IIA).

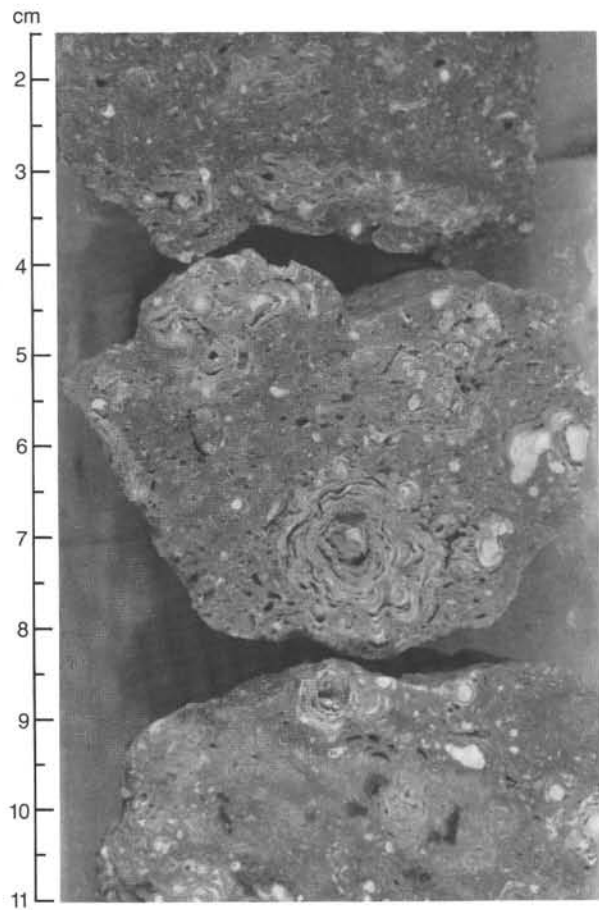


Figure 14. Calcareous dolomite showing calcitic, oncolithic algae embedded in a dolomitic matrix. Upper part shows shell layers; Unit II (Section 117-726A-19X-1, 1-11 cm, Facies IIB).

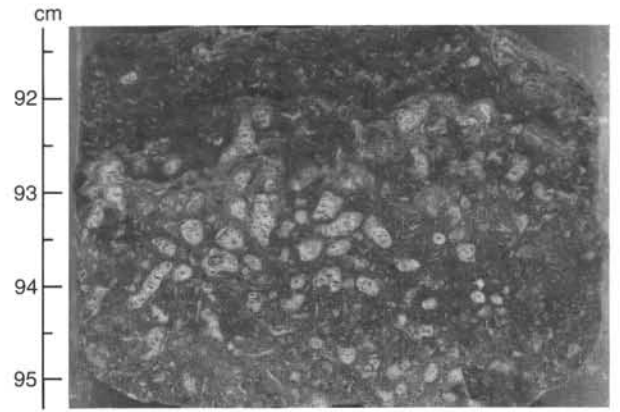


Figure 15. Calcareous, dolomitic wackestone that contains redeposited branches of red algae (calcitic). The matrix of the rock is dolomitized; Unit II (Section 117-726A-19X-1, 91-96 cm, Facies IIB).

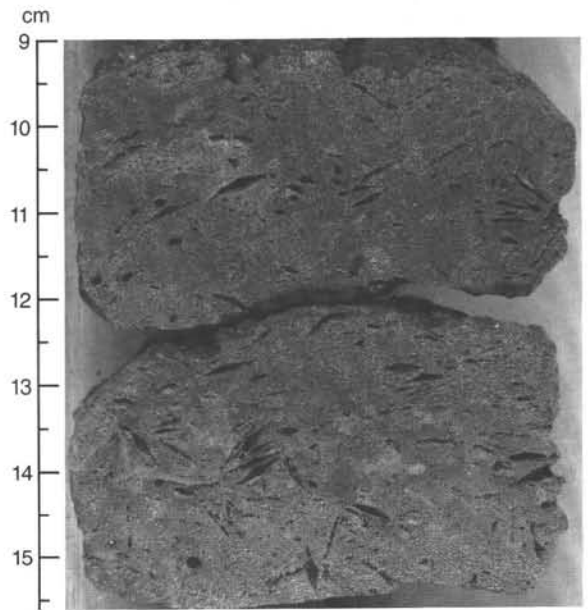


Figure 16. Biomoldic dolomite with molds of foraminifers that locally display a rim of calcite spar; Unit II (Section 117-726A-15X-1, 9-16 cm, Facies IIC).

2. The alternation between bioturbated lag deposits and non-bioturbated to sparsely bioturbated, organic-rich sediments may indicate repeated, drastic changes in the environment at Site 726. Explanations might include oscillations of the top of the oxygen-minimum zone, fluctuations in the intensity of oxygen depletion, sea-level variations, or the development of counter-currents in the upwelling system.

3. Laminated and sparsely bioturbated sediments that lack intercalated lag beds occur between Cores 117-726A-6H and 117-726A-8X (50.9-65.1 mbsf). These sediments, which include the Pleistocene/Pliocene boundary, may indicate a period characterized by a relatively stable and well-developed oxygen-minimum zone (see also Sites 723, 724, and 725 chapters).

**BIOSTRATIGRAPHY**

The recovered section at Site 726 ranges from Holocene to Eocene (?) in age. A pronounced hiatus separates the upper Mi-

ocene from the Eocene (?). The carbonate complex recovered at the bottom of the hole contains probable Eocene (?) species of the benthic foraminiferal genus *Nummulites* and the solely Eocene genus *Actinocyclus*. A plot of faunal datum levels and paleomagnetic reversals vs. depth below the seafloor is presented in Figure 17; for a detailed list of these data points, see Table 3.

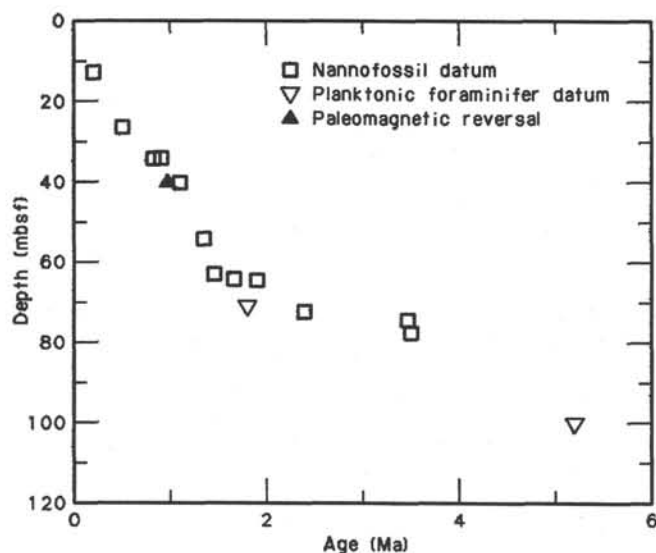


Figure 17. Age-depth plot for Hole 726A. For a detailed list of events, see Table 3.

## Planktonic Foraminifers

Planktonic foraminifers were studied in core-catcher samples of Hole 726A. The upper part of the recovered section (Sections 117-726A-1H through 117-726A-7H, CC; 6.9–63.6 mbsf) consists of pelagic, calcitic, clayey silt and contains common to abundant planktonic foraminifers and highly diverse assemblages. The state of preservation is moderate to good. Below this level, foraminifers are sparse, and preservation of the tests is poor. No small foraminifers were found in the basal part of the section (Sections 117-726A-17X, CC through 117-726A-22X, CC; 154.1–186.3 mbsf), which is composed of shallow-water carbonates of Eocene age.

The upper part of the sequence was referred to Zones N22 and N23, which indicate a Pleistocene age. The lower limit of Zone N23 was found in Sample 117-726A-3H, CC (25.8 mbsf) because this sample contains *Globigerinella calida calida* specimens. The lower limit of Zone N22, which corresponds to the Pleistocene/Pliocene boundary, was placed between Samples 117-726A-7X, CC and 117-726A-8X, CC (63.6–73.2 mbsf) because the latter sample contains obvious Pliocene species, such as *Globoquadrina altispira* and *Globorotalia limbata*. Zones N19 and N20 could not be discriminated from Zone N21, as *Globorotalia tosaensis* is not present in the lower Pleistocene and upper Pliocene sediments. The lower boundary of Zones N19 and N20 was tentatively placed between Samples 117-726A-9X, CC and 117-726A-10X, CC (82.8–92.4 mbsf) because *Sphaeroidinella dehiscens immatura* specimens could not be found in the latter sample.

Below this level *Globorotalia tumida tumida* disappears, which justifies the referral to Zone N17. We made no attempt to

Table 3. Stratigraphic list of faunal events and paleomagnetic reversals for Hole 726A.

Event	Core level	Depth (mbsf)	Age (Ma)	Source of age	Notes
B <i>Emiliana huxleyi</i>	2H-3, 118–119	11.08	0.19	3	
T <i>Pseudoemiliana lacunosa</i>	3H, CC	25.08	0.49	3	
T <i>Reticulofenestra</i> sp. A	4H-1, 118–119	26.98	0.82	3	
B <i>Gephyrocapsa parallela</i>	4H-5, 118–119	32.98	0.89	4	*North Atlantic data.
T <i>Gephyrocapsa</i> *"large"	4H, CC	35.30	1.10	4	*North Atlantic data.
B Jaramillo	5H, CC	44.70	1.10	4	**Long axis greater than 6 $\mu$ m.
T <i>Helicosphaera sellii</i>	5H-3, 45–47	38.75	0.98	6	
B <i>Gephyrocapsa</i> *"large"	5H-3, 115–117	39.45	0.98	6	
T <i>Calcidiscus macintyreii</i>	6H-5, 118–119	51.88	1.36	4	*North Atlantic data.
B <i>Gephyrocapsa</i> *"large"	6H, CC	54.10	1.36	4	*Long axis greater than 6 $\mu$ m.
T <i>Discoaster brouweri</i>	7X-1, 118–119	55.28	1.36	4	*Long axis greater than 6 $\mu$ m.
T <i>Globigerinoides extremus</i>	7X-5, 118–119	61.28	1.45	6	
T <i>Discoaster pentaradiatus</i>	7X, CC	63.60	1.66	4,8	*North Atlantic age consistent with Italian-type section.
T <i>Sphenolithus abies</i>	8X-1, 118–119	64.78	1.9	6	
T <i>Reticulofenestra pseudoumbilica</i>	8X-1, 118–119	64.78	1.9	6	
B <i>Globorotalia tumida tumida</i>	8X-4, 65–67	68.75	1.80	6	* <i>G. obliquus extremus</i> in Berggren et al., 1985.
T <i>Discoaster pentaradiatus</i>	8X, CC	73.20	2.4	6	
T <i>Sphenolithus abies</i>	8X-5, 103–104	70.63	2.4	6	
T <i>Reticulofenestra pseudoumbilica</i>	8X, CC	73.20	3.47	6	
T <i>Sphenolithus abies</i>	8X, CC	73.20	3.47	6	
T <i>Reticulofenestra pseudoumbilica</i>	9X-1, 118–119	74.38	3.5	6	
T <i>Reticulofenestra pseudoumbilica</i>	9X-3, 92–93	77.12	3.5	6	
T <i>Reticulofenestra pseudoumbilica</i>	9X-4, 15–16	77.85	3.5	6	
B <i>Globorotalia tumida tumida</i>	11X-4, 65–67	97.55	5.20	6	
B <i>Globorotalia tumida tumida</i>	11X, CC	102.10	5.20	6	

Note: T = upper limit and B = lower limit. Sources of age are 3 = oxygen isotope data for Site 723 (N. Niitsuma, unpubl. data); 4 = Takayama and Sato, 1987; 6 = Berggren et al., 1985; 8 = Sato et al., in press.

distinguish Zones N16 and N17 as only sparse specimens of upper Miocene *Globorotalia tumida* subspecies were found.

### Benthic Foraminifers

Benthic foraminiferal fauna was studied at Site 726 in the core-catcher samples of Hole 726A. Core-catcher Samples 117-726A-15X, CC (140.7 mbsf) and 117-726A-19X, CC through 117-726A-21X, CC (173.7–183.8 mbsf) contain lithified limestone. Thus, studies of thin sections are required to determine the foraminiferal fauna at the species level.

Benthic foraminiferal fauna at this site varies considerably in its diversity, as well as in its state of preservation. Abundance is high throughout the sequence, except for the sample located just above the limestone (Sample 117-726A-14X, CC; 131.1 mbsf), which contains only a few benthic foraminifers. Preservation is good in the uppermost sample, but becomes moderate by Sample 117-726A-2H, CC (16.3 mbsf). This coincides with the appearance of phosphoritized teeth and vertebrae. The phosphorite becomes nodular in Sample 117-726A-7X, CC (63.6 mbsf). Preservation of benthic foraminiferal tests becomes poor in Sample 117-726A-11X, CC (102.1 mbsf), and the size fraction analyzed through Sample 117-726A-14X, CC (131.1 mbsf) is strongly dominated by crystalline carbonate fluorapatite,  $[Ca_5F(PO_4)_3]$ . A correlation exists between the state of preservation and the amount of phosphorite present. In samples with many phosphoritized teeth and vertebrae, the preservation deteriorates and the abundance decreases. Only occasionally are phosphoritized foraminifers found.

Three samples from within the limestone (117-726A-16X, CC through 117-726A-18X, CC; 148.1–164.1 mbsf) are semilithified; benthic foraminifers have been affected by calcitic recrystallization.

The planktonic/benthic (P/B) ratio at this site is highly variable; it decreases gradually from about 75% in Sample 117-726A-1H, CC (6.9 mbsf) to about 10% in Sample 117-726A-5H, CC (44.7 mbsf). The ratio increases to more than 75% in Samples 117-726A-6H, CC (54.1 mbsf) and 117-726A-7X, CC (63.6 mbsf); and finally decreases to a value below 10% in the remaining samples (below 63.6 mbsf).

Three different assemblages of benthic foraminifers can be recognized at Site 726. The first assemblage (I) is found in the upper part of the sequence (Samples 117-726A-1H, CC through 117-726A-7X, CC; 6.9–63.6 mbsf). Abundant species are *Bolivina ordinaria*, *Cancris* sp. A, *Cibicides wuellerstorfi*, *Hyalina balthica*, and *Uvigerina peregrina*.

The second assemblage (II) found in Samples 117-726A-8X, CC through 117-726A-14X, CC (54.1–131.1 mbsf) yields high abundances of *Bolivina* sp. A., *Lenticulina calcer*, and *Lenticulina* sp. C, as well as some species found in assemblage I (*B. ordinaria* and *U. peregrina*).

The transition from assemblage I to assemblage II occurs somewhere within Core 117-726A-8X (63.6–73.2 mbsf) and coincides with a significant decrease in the P/B ratio (from about 90% planktonic foraminifers to less than 10%). Phosphoritized bones occur in most parts of the sequence, whereas phosphorite in nodular form occurs only in the basal part of benthic foraminiferal assemblage I. Crystalline carbonate fluorapatite occurs only in the basal part of benthic foraminiferal assemblage II, where the P/B ratio is low.

A third assemblage (III) is found in the limestone samples studied (Samples 117-726A-16X, CC through 117-726A-18X, CC; 148.1–164.1 mbsf). These yielded abundant specimens of *Nummulites* spp. Species recognized are *N. cf. planulatus* and *N. cf. pratti*, which are both Eocene. The presence of specimens of the genus *Actinocyclus* in a thin section from Sample 117-

726A-16X, CC (148.1 mbsf) confirms this age because this genus only occurs during the Eocene.

### Calcareous Nannofossils

Calcareous nannofossil floras from Hole 726A, which was the only hole drilled at this site, range from fairly abundant in the upper part to barren in the weakly cemented, partially dolomitized limestone below 140.7 mbsf.

Sediments from the mud line to 11.08 mbsf contain *Emiliania huxleyi* and can be correlated with Zone NN21 (Holocene to Pleistocene). Below Zone NN21, sediments from 11.08 to 25.8 mbsf are placed in Zone NN20 (Pleistocene) because both *E. huxleyi* and *Pseudoemiliania lacunosa* are absent. Underlying sediments from 25.8 to 63.6 mbsf contain *P. lacunosa* and no discoasters, which places these sediments in Zone NN19 (Pleistocene to uppermost Pliocene).

The Pleistocene/Pliocene boundary is located between 63.60 and 64.78 mbsf (between Samples 117-726A-7X, CC and 117-726A-8X-1, 118–119 cm). *Discoaster brouweri* is the only representative of the genus in Samples 117-726A-8X-1, 118–119 cm, down to 117-726A-8X-5, 103–104 cm (64.78–70.63 mbsf). There appears to be a hiatus just below the Pleistocene/Pliocene boundary. The top of *Discoaster pentaradiatus*, which marks the boundary between Zones NN18 and NN17, occurs between Samples 117-726A-8X-5, 103–104 cm, and 117-726A-8X, CC (70.63–73.20 mbsf).

*D. surculus* is extremely rare in the hole, and the sediments ranging from 73.2 mbsf to 77.12 mbsf were tentatively placed in Zones NN17 to NN16 (Fig. 18). The top of *Reticulofenestra pseudoumbilica* occurs between Samples 117-726A-9X-3, 92–93 cm, and 117-726A-9X-4, 15–16 cm. (77.12–77.85 mbsf). This marks the NN16/NN15 zonal boundary.

The sediments from 77.85 mbsf down to 92.4 mbsf were placed in Zones NN15 to NN12, although age-diagnostic species, such as *Amaurolithus tricorniculatus* and *Ceratolithus rugosus* are absent. Underlying sediments from 92.4 to 102.1 mbsf are characterized by comparatively abundant and well-preserved discoasters, such as *D. brouweri*, *D. pentaradiatus*, *D. variabilis*, *D. surculus*, *D. quinquerramus*, and *D. berggrenii*, and belong to Zone NN11. Sediments from 102.1 to 131.1 mbsf contain no age-diagnostic species. Based on the absence of *Discoaster quinquerramus*, however, these sediments were tentatively

Core	Sample	Epoch	Calcareous nannofossils	Radiolarians	Planktonic foraminifers	
0	1	Holocene-Pleistocene	NN21	Barren	N23	
	2		NN20			
	3		NN19		Spongaster pentas	N19-21 N18
	4					
	5					
	6		Pliocene		NN17-16	Barren
	7	NN15-12				
	8	NN11		N16-17		
	9					
100	10	Miocene	NN10	Barren		
	11					
	12					
	13	Eocene (?)	Barren	Barren		
	14					
	15					
	16					
	17					
	18					
	19					
	20					
	21					

Figure 18. Correlation of planktonic microfossil zones in Hole 736A.

placed in Zone NN10. Calcareous nannofossils are completely absent in the remaining sedimentary sequence.

### Radiolarians

Radiolarians are absent from most of the sedimentary sequence recovered at Site 726, except for the interval between Samples 117-726A-8X-2, 85-87 cm, and 117-726A-9X, CC (65.9-82.8 mbsf). In these sediments, there is a good, well-preserved radiolarian fauna belonging to the *Spongaster pentas* Zone, but species diversity is low. Sponge spicules and diatoms are also common in this interval.

### Paleoenvironmental Implications

The Miocene and Pliocene sediments at this site are characterized by frequent lag deposits interbedded with hemipelagic sediments. The sedimentation rate is less than 15 m/m.y., and there is abundant phosphorite. We believe this indicates current winnowing. We suggest that during periods of low sea level, the fine-grained fraction of the sediment eroded away, concentrating the phosphorite initially into coarse-grained sediments and ultimately into nodular deposits (Baturin, 1971; Burnett, 1977). The very low P/B ratio is a further indication of shallow water. The sudden increase in the sedimentation rate (to about 45 m/m.y.) in the Pleistocene together with an increasing P/B ratio suggest a significant deepening of this site, either from eustatic sea-level changes, tectonic activity, or a significant change in climatic conditions. The major part of this subsidence took place during the uppermost Pliocene, but may have been initiated much earlier. The Eocene (?) limestone contains nummulitids and indicates that it was deposited in a shallow-water (less than 200 m) environment.

### PALEOMAGNETISM

Site 726 is located at 17°49'N, 57°22'E in a water depth of 331 m on the Oman margin. Hole 726A was cored to 186.3 mbsf; the lithology consisted of nannofossil-rich calcitic clay to clayey silt (Unit I) and dolomitic limestone (Unit II).

### Magnetic Measurements

Paleomagnetic measurements were conducted on discrete samples using the Minispin magnetometer and the Schonstedt alternating-field (AF) demagnetizer. Detailed research on the stability of the samples during AF demagnetization will be made during post-cruise studies. However, some step-wise AF demagnetizations were performed on specimens from Cores 117-726A-5H and 117-726A-7X and 117-726A-8X. Some of these (Figs. 19 through 21) show quite stable behavior with convex intensity demagnetization curves and median destructive fields up to about 15 mT.

Most of the specimens were AF demagnetized at a blanket AF field of 10 mT. Over the more weakly magnetized intervals of the section, we used a field of 5 mT. Figure 22 shows plots of declination, inclination, and intensity after AF demagnetization. Only specimens with circular standard deviation values of less than 40 are plotted. Over the interval 0 to 40 mbsf, the intensities are relatively uniform and average about 0.2 mA/m. Between about 40 and 70 mbsf, intensities fluctuate from about 0.1 to 5 mA/m, and between about 70 and 100 mbsf, they are more uniform and average about 0.2 mA/m. The sediments below about 100 mbsf were too weakly magnetized to measure. The arithmetic mean intensity is 0.7 mA/m.

### Magnetostratigraphy

Although inclination values correspond well to the expected axial dipole values (Fig. 23), correlation of the paleomagnetic record at Site 726 with the polarity time scale is not straightforward. Ignoring isolated points, the section is normally magnetized down to about 39 mbsf, and then reversely magnetized to

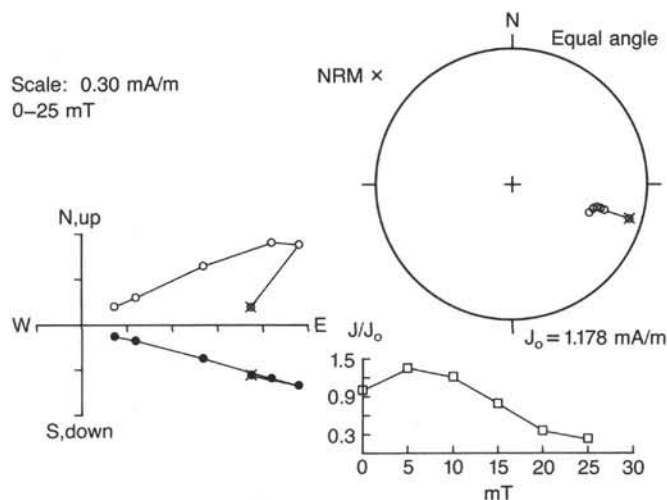


Figure 19. Results of step-wise AF demagnetization of discrete specimen from Hole 726A.

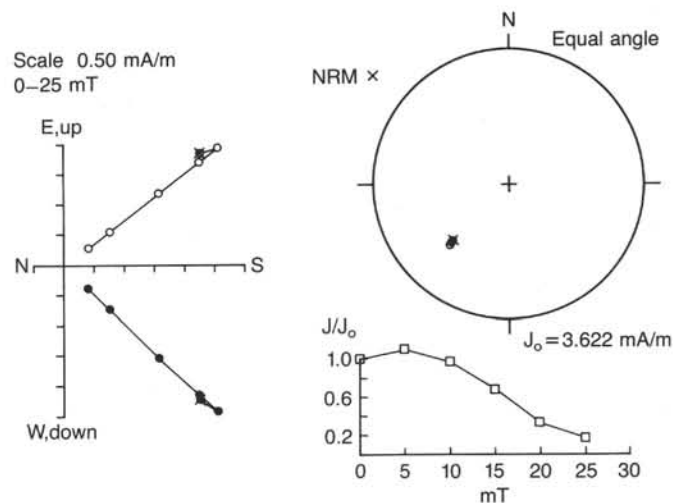


Figure 20. Results of step-wise AF demagnetization of discrete specimen from Hole 726A.

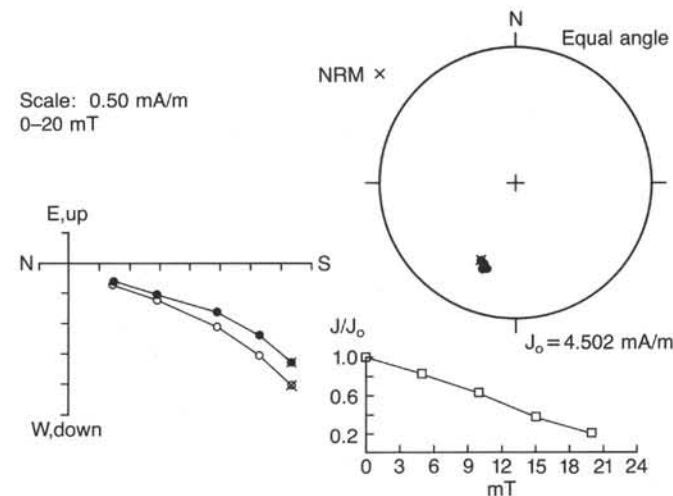


Figure 21. Results of step-wise AF demagnetization of discrete specimen from Hole 726A.

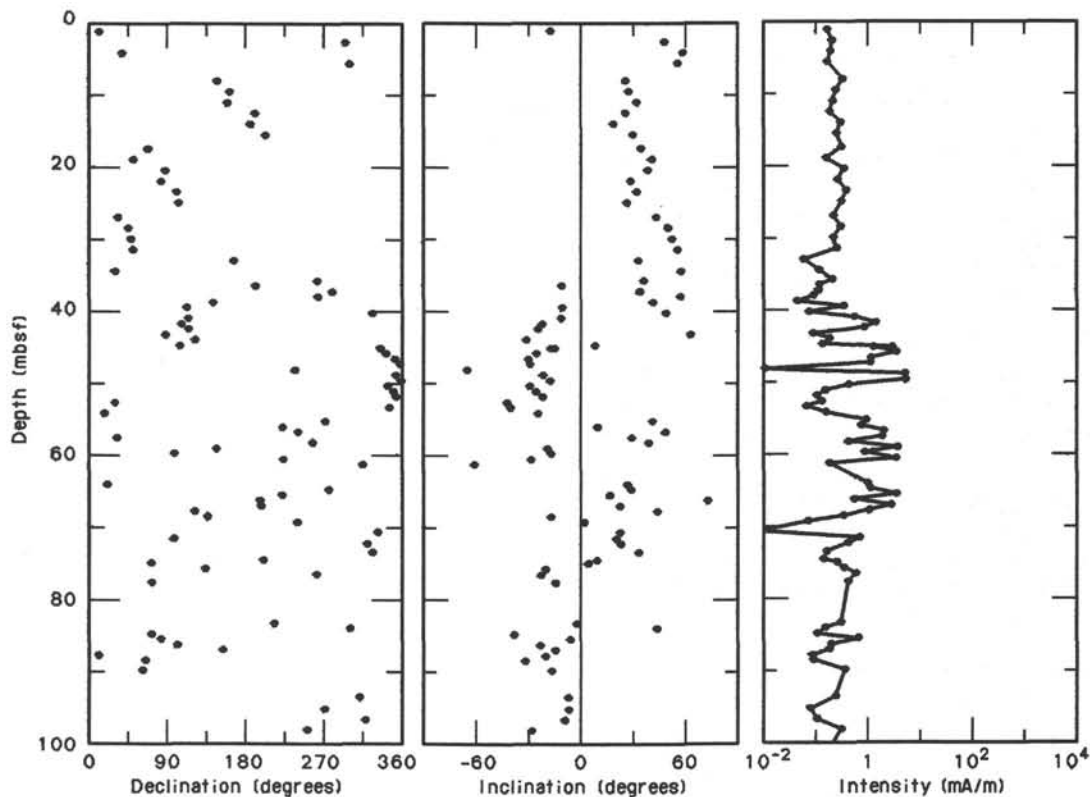


Figure 22. Declination, inclination, and intensity after AF demagnetization of discrete specimens from Hole 726A.

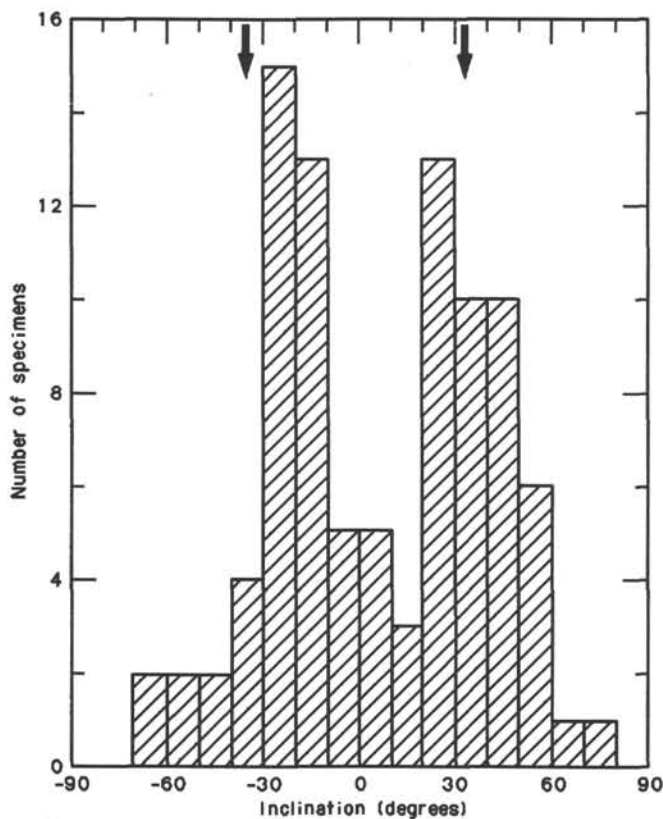


Figure 23. Inclination values grouped into 10° classes for discrete specimens from Hole 726A. Arrows indicate values expected from geocentric axial dipole field.

about 55 mbsf. A series of well-defined polarity transitions occurs between 55 and about 75 mbsf; between 75 and 100 mbsf, the section is reversely magnetized. The nannofossil stratigraphy (see "Biostratigraphy" section, this chapter) shows that the top of acme *Reticulofenestra* sp. A and the first appearance datum (FAD) of *Gephyrocapsa parallela* occur within Core 117-726A-4H (25.8–35.3 mbsf). Although both of these datums significantly predate the Chron C1/C1r (Brunhes/Matuyama Chronozone) boundary (Takayama and Sato, 1987), we find no suggestion of a polarity transition above the base of Core 117-726A-4H. Therefore, we tentatively assigned the transition at 39 mbsf (between intervals 117-726A-5H-3, 45 cm, and 117-726A-5H-3, 115 cm) to the bottom of Subchron C1r-1 (Jaramillo Subchronozone).

The FAD of *Gephyrocapsa oceanica* and the last appearance datum (LAD) of *Discoaster brouweri*, respectively, approximate to the upper and lower boundaries of Chron C2 (Olduvai Subchronozone; Takayama and Sato, 1987). These datums occur within Core 117-726A-8X (63.6–73.2 mbsf) and do coincide roughly with the upper and lower boundaries of a normally magnetized interval. However, interpretation of the normally magnetized interval between about 55 and 60 mbsf then becomes difficult because the only well-documented potential subchron corresponding approximately to this time interval is the Cobb Mountain Subchronozone, which may have lasted for only about 0.02 m.y. (Clement and Robinson, 1987). For this reason, we are reluctant to correlate any of the normally magnetized intervals within this part of the section with the polarity time scale. Nannofossil Zones NN18 to NN11 were placed within Cores 117-726A-8X to 117-726A-11X (63.6–102.1 mbsf). Therefore, the reversely magnetized interval below about 75 mbsf corresponds in time to several normal and reversed chrons, and for this reason we were reluctant to correlate it with the reversal time scale.

The only available evidence that might explain the anomalous paleomagnetic record below about 50 mbsf is the sugges-

tion of increased influence of current-controlled deposition, in the form of several lag deposits, which begin in Core 117-726-4H (see "Lithostratigraphy" section, this chapter). Although we avoided obvious lag deposits during sampling, an overall coarsening of the terrigenous (and magnetic) fraction as a result of winnowing could be one explanation for failure of the sediments to preserve an interpretable paleomagnetic record over this interval. However, this does not agree with the stable behavior of several specimens from this interval during AF demagnetization.

### Magnetic Susceptibility

The volume magnetic susceptibility of Hole 726A sediments was measured using Bartington Instruments whole-core sensor at the 0.1 sensitivity and low-frequency (0.47 kHz) settings. Hole 726A was cored in the APC mode to Core 117-726A-6H (54.1 mbsf); drilling then continued in XCB mode to Core 117-726A-22X (186.3 mbsf).

Two lithologic units were encountered. Lithologic Subunit IA, a marly nanfossil ooze, extends from the surface to ~32 mbsf and is characterized by low susceptibility values ( $40$  to  $90 \times 10^{-6}$  volume SI units), compared to the other Oman margin sites (Fig. 24). Lithologic Subunit IB (32–131.1 mbsf) contains alternating layers of organic-rich silty clay and foraminiferal sand. The susceptibility values of Unit IB are slightly lower than those of Unit IA. Toward the base of Unit IB, susceptibility values are consistently negative ( $-15 \times 10^{-6}$  volume SI units) and natural remanent magnetization (NRM) intensities approach the noise level of the instrument, indicating the virtual disappearance of ferrimagnetic particles and the predominance of diamagnetic components. We are uncertain whether this condition is of depositional or diagenetic origin. However, the chemical data for this hole do not reveal any clear gradients at this level. Smear slide and carbonate analyses over the 110 to 120 mbsf interval indicate increasing percentages of biogenic carbonate and euhedral dolomite, which suggests that these components may be the cause of the diamagnetism (see "Lithostratigraphy" and "Inorganic Geochemistry" sections, this chapter). The calculated volume magnetic susceptibility of a sample of pure calcite (or dolomite) is  $\sim 13 \times 10^{-6}$  volume SI units. Lithologic Unit II, which consists of dolomitic limestone, was observed from ~130 mbsf to the base of Hole 726A. Carbonate analyses on these sediments often exceeded 100% because of the effect of dolomite. Although recovery of lithologic Unit II was poor, the measured susceptibilities were commonly negative, which presumably also reflects the diamagnetism of calcium carbonate and dolomite.

Detailed correlations between Hole 726A and other Oman margin sites were difficult to establish. The nanfossil biozonations of Hole 726A indicate that the Brunhes/Matuyama Chronozone boundary should be positioned at about 30 mbsf (see "Biostratigraphy" section, this chapter). Using this tentative chronostratigraphic datum, Hole 726A data may be compared with the well-defined Brunhes Chronozone susceptibility data from Hole 723B (Fig. 25). Although gross similarities of the two profiles are apparent, detailed correlations between sites are generally not possible. No obvious correlations of Hole 726A with other Oman margin sites were apparent below the Brunhes Chronozone.

### ACCUMULATION RATES

At Site 726, magnetostratigraphic and biostratigraphic data were used to determine sedimentation rates for the top 100 m of sediment (most of lithologic Unit I). Rates over the last 3.5 m.y. were calculated between nanfossil datums where ages were determined from oxygen-isotope stratigraphy (Niitsuma, unpubl. data; Berggren et al., 1985; Table 3). For the last 1.45 m.y., the mean rate varied between 24 and 66 m/m.y., with an average of

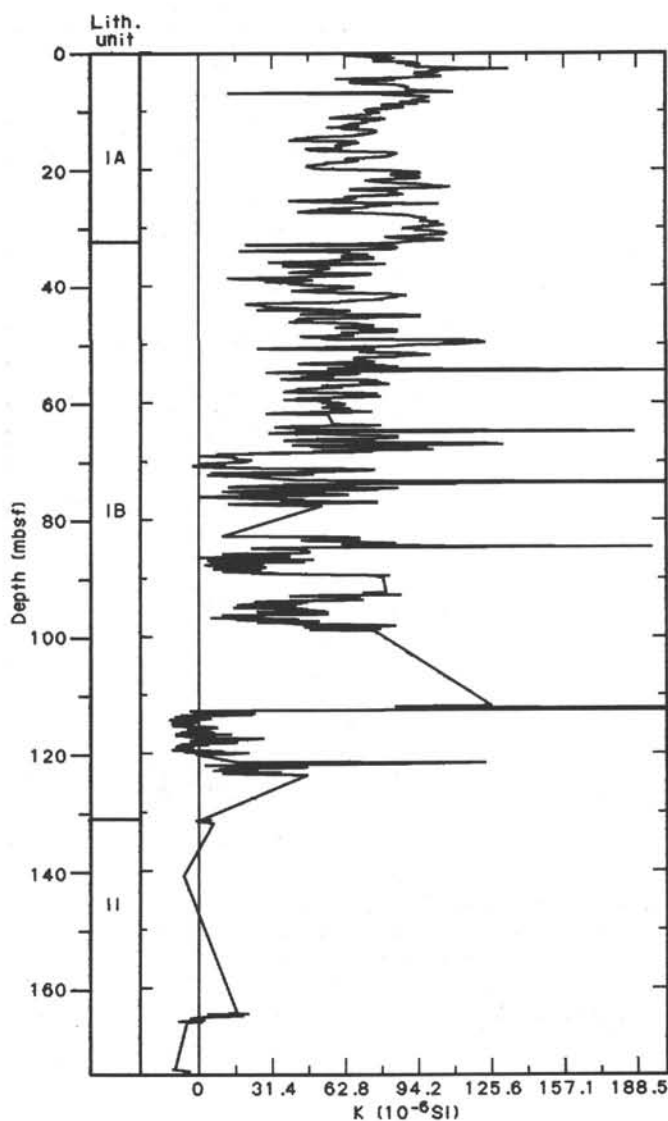


Figure 24. Whole-core, magnetic-susceptibility stratigraphy for Hole 726A.

45 m/m.y. These rates are the lowest measured in the upper slope basin and are similar to those found in pelagic deposits on the Owen Ridge (see Owen Ridge site chapters, this volume). The higher mean sedimentation rate near the top of Site 726 (Fig. 26) corresponds to the sediments containing abundant small shell fragments and more foraminifer shells than in older sediments of lithologic Subunit IA (see "Lithostratigraphy" section, this chapter).

A hiatus, which represents about 450,000 yr of missing sediment accumulation, is located near 63 mbsf (Fig. 26). Below this level, sediments are characterized by coarse-grained lag deposits interbedded with organic-carbon-rich, nanfossil-foraminifer oozes. In accordance with periods of nondeposition and winnowing, the average sedimentation rate is a factor-of-three lower than rates in more recent deposits (15 vs. 45 m/m.y.).

The mass accumulation of calcium carbonate, organic carbon, and noncarbonate sediment components is calculated from average values between the nanoplankton datum levels (Table 4; Fig. 27). The accumulation of calcium carbonate and noncar-

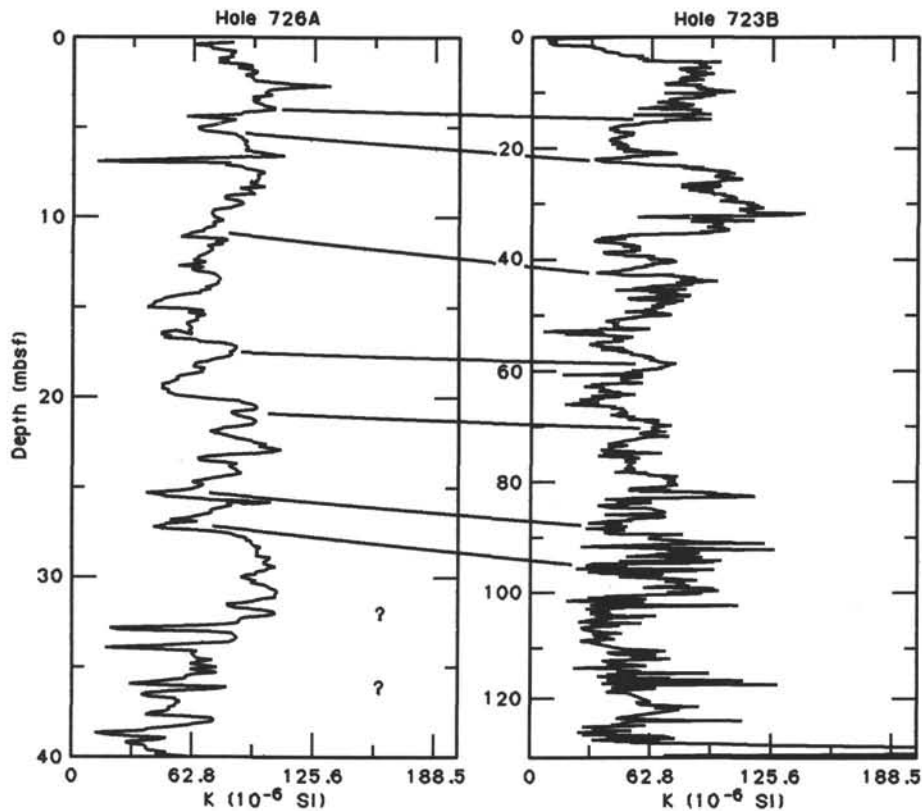


Figure 25. Possible correlation of magnetic susceptibility features between Holes 726A and 723B.

bonate increase upsection, following the sedimentation rate changes. Organic carbon concentrations and accumulations are greatest near the Pleistocene/Pliocene boundary. Similar concentrations of organic carbon in the late Pliocene and early Pleistocene have been observed at other Oman margin sites (i.e., see Sites 723 and 724 chapters, this volume), which suggests a regional change in organic carbon production and/or preservation at this time.

## PHYSICAL PROPERTIES

### Introduction

Physical-properties measurements at Site 726 included index properties (wet-bulk density, grain density, porosity, and water content), wet-bulk densities determined using the GRAPE, and compressional-wave velocities determined with the *P*-wave logger (PWL). Measurements using the GRAPE and PWL systems were conducted on cores that were sufficiently coherent and at least 80 cm long. In addition, wet-bulk densities measured using GRAPE special 2-min counts were performed on discrete samples taken from the dolomite and limestone recovered from lithologic Unit II. Compressional-wave velocities were measured on discrete samples beginning at Core 117-726A-15X using the Hamilton Frame. Compressional-wave data were not collected in the cores preceding Core 117-726A-15X because the gas-induced expansion of the sediment resulted in a poor signal transmission. Vane shear strengths were not measured because the sediments were coarse-grained and sufficiently indurated to preclude using the Wykeham-Farrance vane shear device. The properties determined at Site 726 are listed in Table 5. All techniques and equipment used are described in the "Explanatory Notes" (this volume).

## Index Properties

### Lithologic Unit I

Lithologic Unit I (0–131.1 mbsf) is divided into two subunits that differ in bulk density, porosity, water content, and grain density. Subunit IA (0–32.1 mbsf) is a calcareous silty clay to marly calcareous ooze that displays nearly constant index properties (Fig. 28). In Subunit IA, porosity averages 53%, water content averages 30%, wet-bulk density averages 1.84 g/cm<sup>3</sup>, and grain density averages 2.67 g/cm<sup>3</sup>.

Subunit IB (32.1–131.1 mbsf) is an organic-rich silty clay and marly nannofossil ooze/chalk, with occasional diatomaceous horizons. The boundary between Subunits IA and IB is marked by an increase in porosity and water content and a decrease in bulk and grain densities (Fig. 28). From the boundary to 36 mbsf, porosity increases from 53% to 63%, water content increases from 30% to 41%, wet-bulk density decreases from 1.84 to 1.61 g/cm<sup>3</sup>, and grain density decreases from 2.68 to 2.46 g/cm<sup>3</sup>. These changes in index properties most likely result from an increase in organic carbon from 1.1% to 3.6% (see "Lithostratigraphy" section, this chapter). The amount of organic carbon remains high to a depth of 70 mbsf. As a result, porosity and water content are high and bulk and grain densities are low to this depth. Abundant diatoms in the interval 60 to 70 mbsf contribute to the high porosity and low densities.

The interval from 70 to 100 mbsf displays trends of decreasing porosity (65%–58%) and water content (41%–34%) and increasing wet-bulk density (1.62 to 1.76 g/cm<sup>3</sup>) and grain density (2.56 to 2.70 g/cm<sup>3</sup>). From 70 to 85 mbsf, these trends probably result from the decrease in organic carbon (2.62% to 1.5%; see "Lithostratigraphy" section, this chapter). However, the interval from 85 to 100 mbsf shows an increase in organic carbon

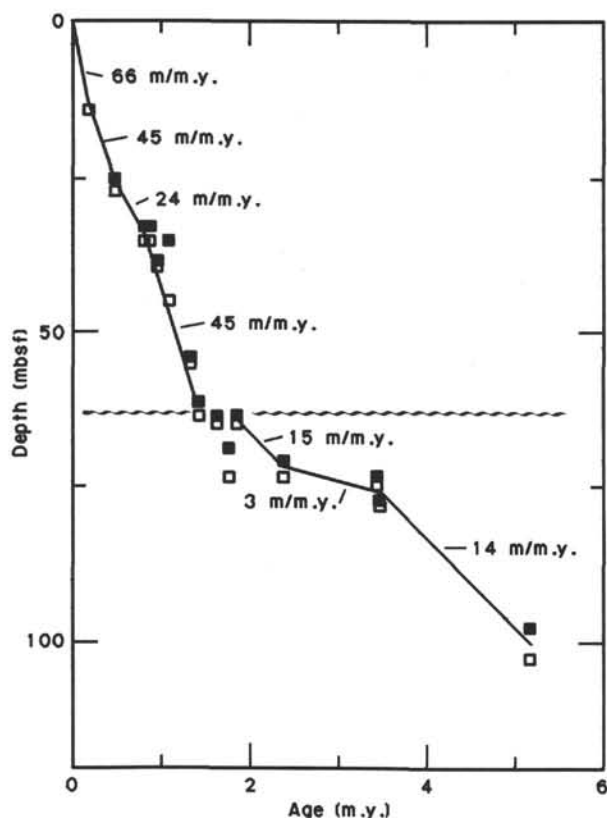


Figure 26. Age-depth plot of stratigraphic datums listed in Table 3. The filled and open boxes represent the upper and lower depths of each datum level, respectively. Indicated sedimentation rates are calculated between reliable nannofossil and foraminifer datum levels.

(1.58% to 3.45%), which suggests that organic carbon content has a diminishing control over physical properties. Porosity and water content decrease and wet-bulk and grain densities increase, between 115 mbsf and the bottom of Unit I (131 mbsf) in response to the increase in dolomite below Core 117-726A-12X.

#### Lithologic Unit II

Unit II (131.1–186.3 mbsf) consists of dolomite and limestone. Wet-bulk densities, from the GRAPE special 2-min counts, steadily increase from 1.98 to 2.76 g/cm<sup>3</sup> as a result of the downsection increase in cementation and dolomitization (see "Lithostratigraphy" section, this chapter).

#### Compressional-Wave Velocities

Compressional-wave velocities were determined on the limestone and dolomite samples recovered from lithologic Unit II.

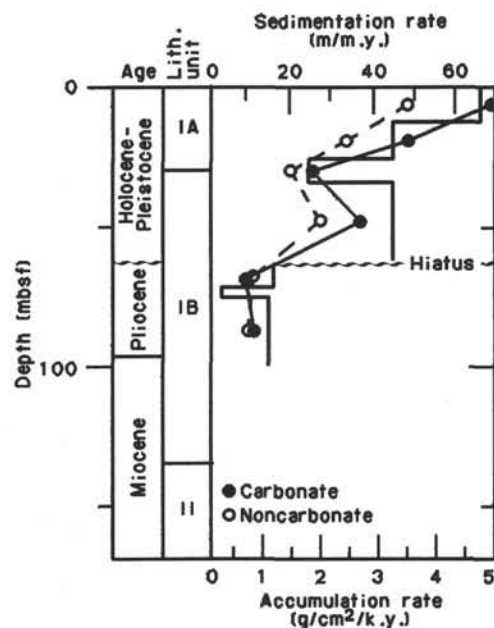


Figure 27. Sedimentation rate (m/m.y.; solid line), calcium carbonate accumulation rate (g/cm<sup>2</sup>/k.y.; closed circles), and noncarbonate accumulation rates (g/cm<sup>2</sup>/k.y.; open circles) vs. depth (mbsf) at Site 726. Accumulation rates are plotted at the midpoint of the respective depth intervals.

Measurements parallel and perpendicular to bedding show that these samples are anisotropic with respect to the direction of propagation of the compressional wave. Velocities measured parallel to bedding are consistently higher than those measured perpendicular to bedding; 4245 to 6134 m/s and 4194 to 5889 m/s, respectively (Table 5). Velocity anisotropies range from 1.2% to 7.1%.

#### GRAPE and P-Wave Logs

GRAPE wet-bulk densities were obtained for Cores 117-726A-1H to 117-726A-14X, which corresponds to lithologic Unit I. The primary factor affecting the quality of the GRAPE data is the degree of core disturbance that resulted from sediment expansion. Quality of data is good to a depth of 80 mbsf and clearly shows the transition between the two subunits in lithologic Unit I. In the first 50 mbsf interval, the data correlate well with the wet-bulk densities measured on the discrete samples (Fig. 29).

P-wave logs were obtained throughout lithologic Unit I (Cores 117-726A-1H through 117-726A-14X; Fig. 30). Below this interval, there was insufficient contact between the sediment and the core liner to provide adequate signal transmission. Although the

Table 4. Sedimentation and accumulation rate data for Site 726.

Depth interval (mbsf)	Age range (m.y.)	CaCO <sub>3</sub> (̄%)	C <sub>org</sub> (̄%)	Dry-bulk density (̄g/cm <sub>3</sub> )	Sed. rate (̄m/m.y.)	CaCO <sub>3</sub> acc. rate (g/cm <sup>2</sup> /k.y.)	Non-CaCO <sub>3</sub> acc. rate (g/cm <sup>2</sup> /k.y.)	C <sub>org</sub> acc. rate (mg/cm <sup>2</sup> /k.y.)
0–12.6	0–0.19	58.7	0.54	1.261	66.3	4.91	3.45	45.1
12.6–26.0	0.19–0.49	59.3	0.49	1.305	44.7	3.46	2.37	28.6
26.0–34.1	0.49–0.82	56.1	1.1	1.305	24.5	1.79	1.40	35.2
34.1–62.4	0.82–1.45	57.6	2.54	1.012	44.9	2.62	1.93	115.4
64.2–71.9	1.90–2.40	45.4	3.32	0.889	15.4	0.62	0.75	45.5
71.9–75.0	2.40–3.48	ND	ND	ND	2.9	ND	ND	ND
75.0–99.8	3.48–5.20	53.3	2.25	1.002	14.4	0.77	0.67	32.5

Note: ND = no data from interval.

Table 5. Physical properties summary for Hole 726A.

Core, section, interval (cm)	Depth (mbsf)	Wet-bulk density (g/cm <sup>3</sup> )	Porosity (%)	Water content (%)	Grain density (g/cm <sup>3</sup> )	Dry-bulk density (g/cm <sup>3</sup> )	Velocity (m/s)
117-726A-							
1H-5, 52-54	6.52	1.849	50.5	28.0	2.639	1.332	
2H-4, 60-62	12.00	1.776	57.1	33.0	2.683	1.190	
2H-7, 60-62	16.50	1.847	52.4	29.0	2.672	1.311	
3H-3, 50-52	19.80	1.760	57.9	33.7	2.625	1.166	
3H-5, 50-52	22.80	1.879	50.7	27.7	2.647	1.359	
3H-7, 50-52	25.80	1.906	51.2	27.5	2.750	1.382	
4H-3, 50-52	29.30	1.841	51.0	28.4	2.624	1.319	
4H-5, 50-52	32.30	1.841	53.0	29.5	2.679	1.297	
4H-7, 30-32	35.10	1.733	58.7	34.7	2.717	1.131	
5H-1, 80-82	36.10	1.606	63.4	40.5	2.456	0.956	
5H-3, 130-132	39.60	1.601	63.9	40.9	2.573	0.946	
5H-5, 52-54	41.82	1.594	67.5	43.4	2.590	0.902	
6H-2, 50-52	46.70	1.681	59.9	36.5	2.555	1.068	
6H-4, 50-52	49.70	1.684	60.8	37.0	2.581	1.062	
6H-6, 50-52	52.70	1.743	58.4	34.3	2.643	1.145	
7X-1, 98-100	55.08	1.572	62.4	40.7	2.409	0.933	
7X-3, 100-102	58.10	1.592	65.5	42.2	2.580	0.921	
7X-5, 100-102	61.10	1.683	61.3	37.3	2.597	1.055	
8X-1, 52-54	64.12	1.469	73.5	51.3	2.485	0.716	
8X-3, 52-54	67.12	1.614	60.6	38.4	2.404	0.993	
8X-6, 27-29	71.37	1.623	65.0	41.0	2.560	0.957	
9X-2, 117-119	75.87	1.517	67.9	45.9	2.641	0.821	
10X-2, 127-129	85.57	1.610	64.2	40.8	2.551	0.953	
10X-4, 31-33	87.61	1.739	59.6	35.1	2.687	1.128	
11X-2, 60-62	94.50	1.609	65.6	41.8	2.619	0.936	
11X-4, 99-101	97.89	1.769	58.4	33.8	2.695	1.171	
13X-3, 130-132	116.10	1.585	69.0	44.6	2.649	0.879	
13X-6, 66-68	119.96	1.913	49.7	26.6	2.709	1.404	
14X-2, 5-7	122.95	1.942	46.5	24.5	2.697	1.466	
15X-1, 41-43	131.51	2.387					<sup>a</sup> 4194 <sup>b</sup> 4245
15X-1, 58-60	131.68	2.326	30.0	13.2	2.760	2.019	
16X, CC 22-24	141.13	1.988	45.5	23.4	2.683	1.522	
17X, CC 30-32	148.40	2.105					<sup>a</sup> 2230
19X-1, 91-93	165.01	2.614					<sup>a</sup> 5388 <sup>b</sup> 5511
20X, CC 37-39	174.72	2.736					<sup>a</sup> 5597 <sup>b</sup> 6009
21X, CC 3-5	183.43	2.758					<sup>a</sup> 5889 <sup>b</sup> 6134

<sup>a</sup> Velocity measurement perpendicular to bedding.

<sup>b</sup> Velocity measurement parallel to bedding.

velocity profile is discontinuous, it correlates with the GRAPE profile. The velocity values obtained with the PWL vary between 1600 and 1650 m/s in Subunit IA and decrease sharply to 1550 m/s in the lower density sediments of Subunit IB.

## INORGANIC GEOCHEMISTRY

Five interstitial-water samples were collected by squeezing at Site 726 and analyzed for alkalinity, pH, salinity, magnesium, calcium, chloride, sulfate, phosphate, ammonia, and silica (Table 6). The Barnes *in-situ* sampler was used once at a depth of 34.8 mbsf, where it collected pristine interstitial water.

### Salinity, Chloride, and pH

The concentration profiles of chloride, salinity, and pH are shown in Figure 31. Both salinity and chloride increase with depth, with salinity being uniformly constant at 36.3 g/kg below 5.95 mbsf. Chloride is ~20 mmol/L greater at the base of Hole 726A than at the top. These chloride concentrations were the highest measured during Leg 117. The chloride maximum at a depth of ~80 m probably results from a different phenomenon than that observed at Sites 724 and 725. At both these latter sites, the maximum occurs in sediments deposited in the middle Pleistocene, whereas sediments at 80 mbsf at Site 726 are much older (at least Pliocene age). We are unable to explain the chloride maximum at this site. The pH shows minimal variation downhole and ranges between 7.93 and 7.55.

### Sulfate and Alkalinity

Unlike other sites investigated during Leg 117, Site 726 is characterized by high sulfate concentrations over the length of the cored section (down to ~118 mbsf). Over this depth interval, sulfate decreases from 26.5 to 25.5 mmol/L, with a minimum of 22.6 mmol/L at 76 mbsf. Alkalinity produced through the oxidation of organic matter is very low and reaches a maximum of 5.63 mmol/L in Core 117-726A-9X at 76 mbsf. There is some indication that the more pronounced decrease in sulfate between 34 to 50 mbsf is responsible for adding 2.7 mmol/L of alkalinity to the pore water over the same interval. The concentration and distribution of alkalinity and sulfate at Site 726 suggest that the sediment is low in labile organic matter, and that the slow accumulation rate of the sediments allows sulfate to diffuse from overlying seawater to depths of up to 50 mbsf. Further evidence for this hypothesis is outlined below. Table 7 and Figure 32 indicate that levels of dissolved organic carbon (DOC) are much lower at this site than at Sites 723, 724, and 725, which is consistent with the proposed interpretation.

### Ammonia, Phosphate, and Silica

Both ammonia and phosphate, products of organic matter degradation, increase with depth, reaching maximum concentrations of 0.69 mmol/L and 8.1 μmol/L at 76 mbsf, respectively. Assuming Redfield stoichiometry for the organic matter, the reduction of ~6 mmol/L of sulfate at Site 726 should produce ~0.9 mmol/L of ammonia and ~45 μmol/L of phosphate. Thus, Figure 31 indicates that little ammonia removal

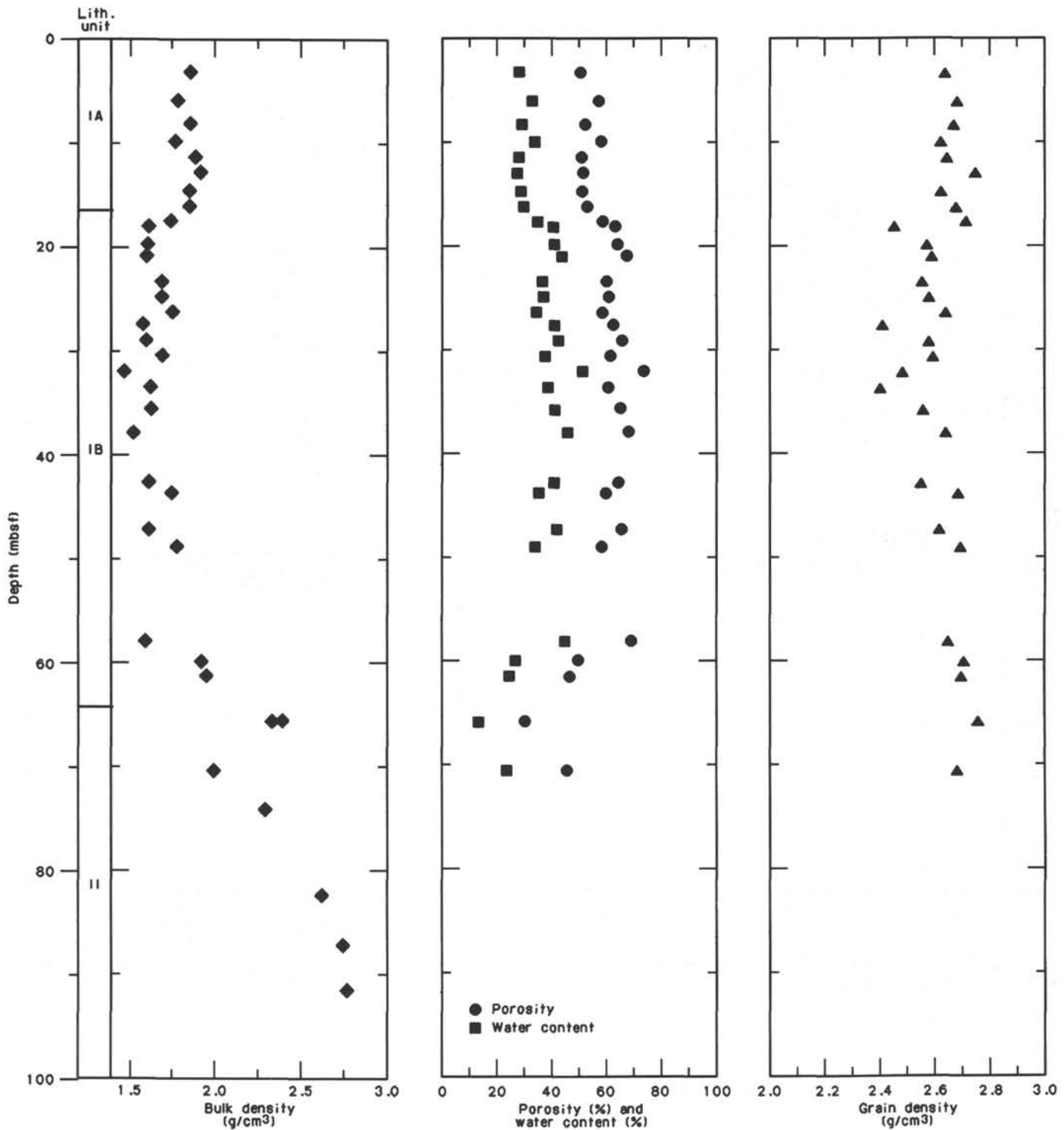


Figure 28. Index properties measured on discrete samples.

onto clays occurs, but phosphate stripping is obvious, in particular over the depth interval from 20 to 40 mbsf. Mineralogical identification (see below) from residues left after sieving for benthic foraminifers reveals large quantities of phosphorite throughout the core. Large nodules and pellets are concentrated at the upper Pliocene unconformity in Section 117-726A-7X, CC. Below 100 mbsf, crystalline carbonate fluorapatite becomes abundant, corresponding to the observed decrease in phosphate below 76 mbsf.

Dissolved silica in the interstitial waters increases from bottom-water values (130-140  $\mu\text{mol/L}$ ) to a maximum of 964  $\mu\text{mol/L}$  at 76 mbsf (Fig. 31). The concentration of silica is less here than at previous sites and may reflect control by two limiting mechanisms. First, the slow accumulation rate allows considerable opal-A solution to occur over the upper few meters of the sediment column, thereby reducing the content of opal available for later dissolution. Second, the level of biogenic silica at this site is low (except in the lower Pliocene, 70-90 mbsf) and in-

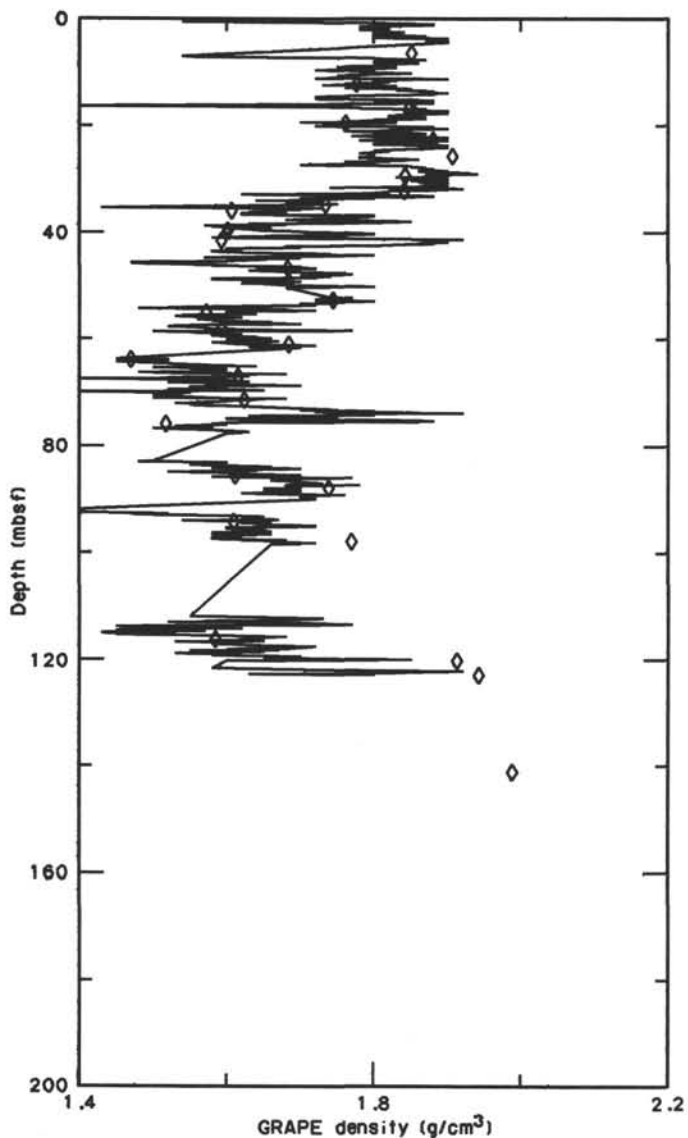


Figure 29. GRAPE wet-bulk density (solid line) and wet-bulk density from discrete samples (diamonds). GRAPE data are 10-cm-block averages.

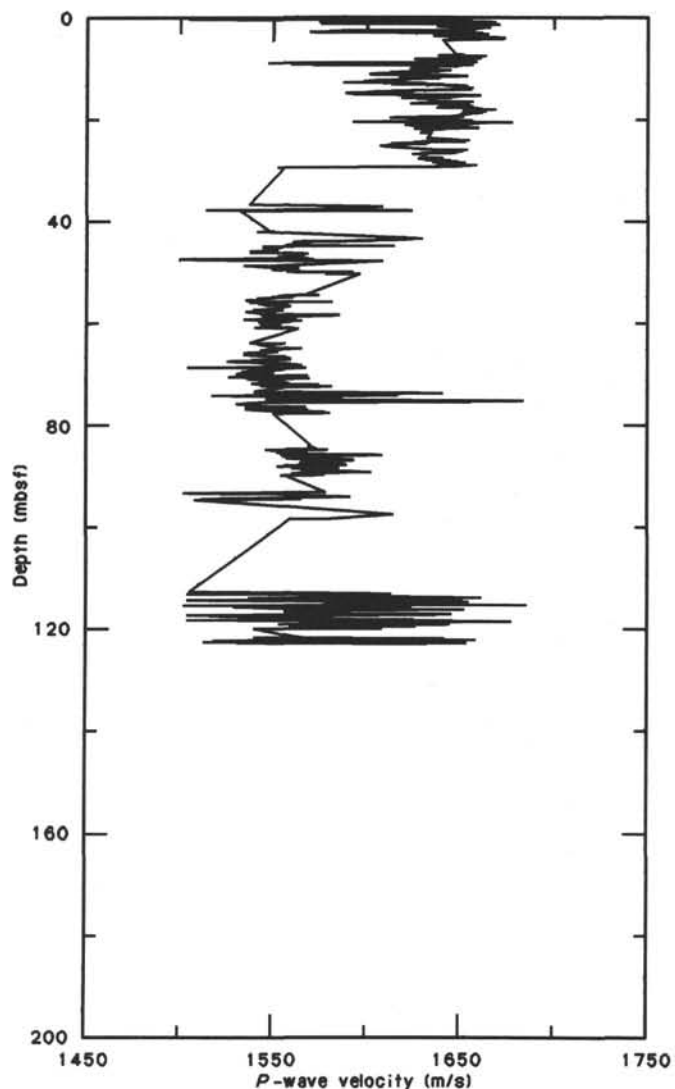


Figure 30. Compressional-wave velocity as measured by the *P*-wave logger.

Table 6. Summary of geochemical data for interstitial water at Hole 726A.

Core, section, interval (cm)	Depth (mbsf)	Vol. (mL)	pH	Alk. (mmol/L)	Sal. (g/kg)	Mg (mmol/L)	Ca (mmol/L)	Cl (mmol/L)	SO <sub>4</sub> (mmol/L)	PO <sub>4</sub> (μmol/L)	NH <sub>4</sub> (mmol/L)	SiO <sub>2</sub> (μmol/L)	Mg/Ca
117-726A-1H-4, 145-150	5.95	41	7.93	4.41	35.8	53.31	11.15	574	26.5	2.1	0.07	147	4.78
117-726A-3H-4, 145-150	22.25	35	7.76	3.04	36.3	50.96	13.42	582	26.4	0.7	0.22	251	3.80
117-726A-4H-7, 0-1	34.80	10	7.80	2.69	36.3	50.71	13.67	588	26.1	1.1	0.27	461	3.71
117-726A-6H-4, 145-150	50.65	41	7.78	5.43	36.3	45.89	15.80	588	22.6	7.0	0.58	885	2.90
117-726A-9X-2, 145-150	76.15	49	7.89	5.63	36.3	45.80	17.00	595	22.59	8.1	0.69	964	2.69
117-726A-13X-4, 145-150	117.75	63	7.55	3.42	36.3	45.90	18.72	593	25.5	2.6	0.21	427	2.45

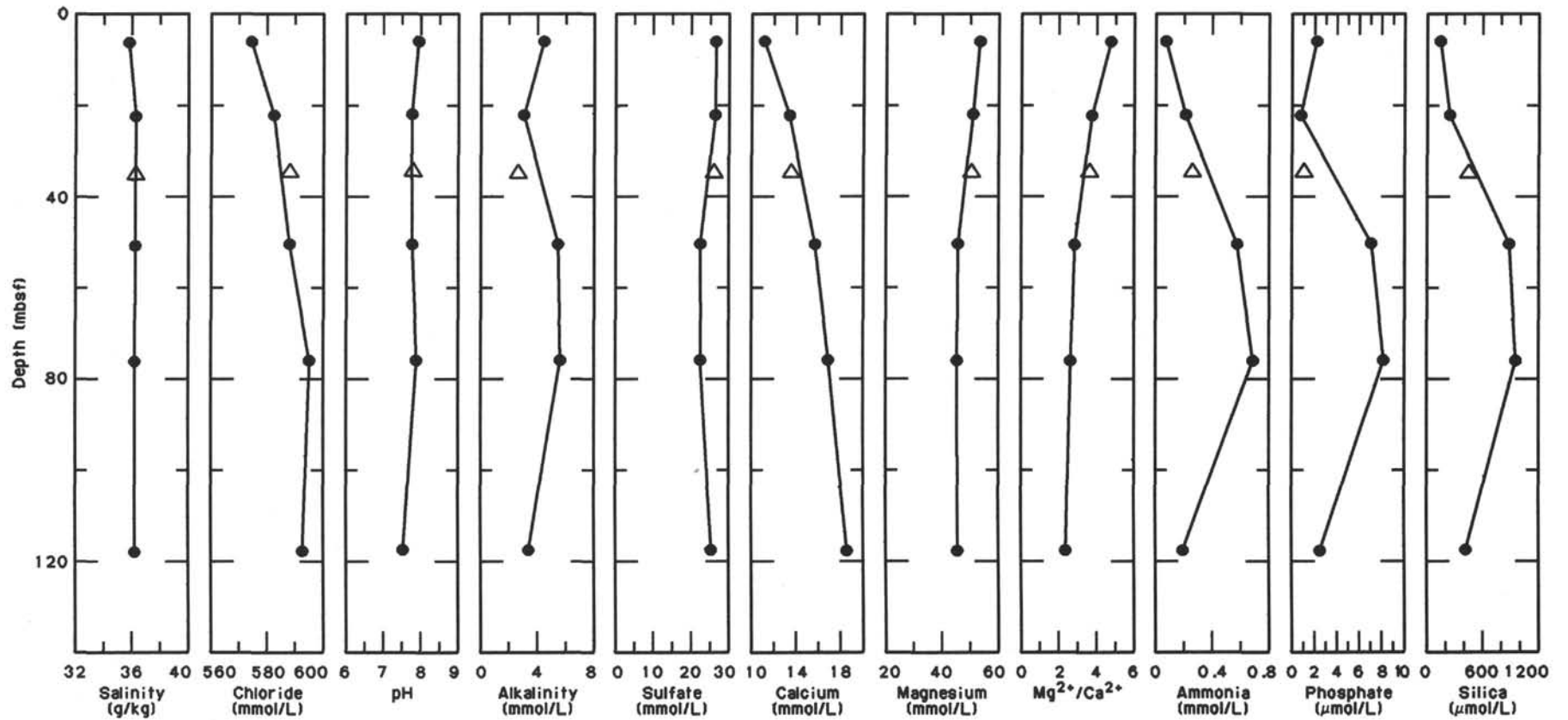


Figure 31. Distribution of concentrations in interstitial waters at Site 726.

**Table 7. Dissolved organic carbon at Site 726.**

Core, section, interval (cm)	Depth (mbsf)	DOC (a.u.)
117-726A-1H-4, 145	5.95	0.097
3H-4, 145	22.25	0.175
4I-7, 1	34.80	0.168
6H-4, 145	50.65	0.393
9X-2, 145	76.15	0.695
13X-4, 145	117.75	0.169

For explanation of parameters given, see "Explanatory Notes" (this volume); a.u. = absorbance units.

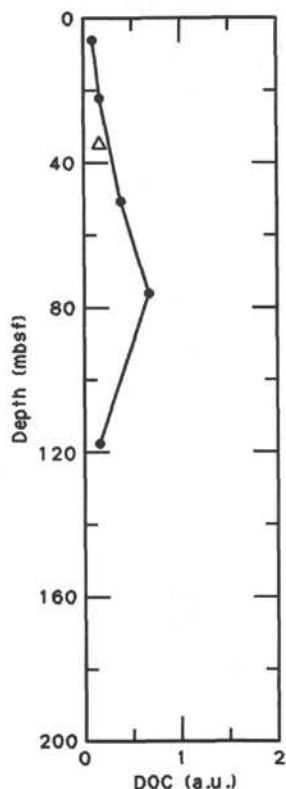


Figure 32. Distribution of dissolved organic carbon (DOC) at Site 726, expressed as absorbance units.

insufficient for dissolution to proceed to equilibrium ( $\sim 1000 \mu\text{mol/L}$ ) with opal at depth.

### Calcium and Magnesium

Profiles of dissolved calcium and magnesium are displayed in Figure 31. Calcium increases from 11.2 mmol/L at  $\sim 6$  mbsf to 18.7 mmol/L at  $\sim 118$  mbsf. Magnesium decreases from 53.3 to 45 mmol/L over the same depth interval, and the profile is vertical below 50 mbsf. This distribution indicates that diffusion is absent, which rules out alteration of basalt as a control of magnesium geochemistry at this site. However, the linear calcium gradient between 50 mbsf and the bottom of the hole indicates that calcium is diffusing upward from an unknown source below the cored section.

The curvature evident in both profiles between 10 and 40 mbsf indicates that the greatest degree of reaction, probably do-

lomitization of preexisting calcite, occurs in this interval. Smear slide descriptions (see "Lithostratigraphy" section, this chapter) indicate abundant dolomite rhombohedra throughout the Pleistocene section.

### Sediment Mineralogy

The distribution of phosphorite at this site is of great interest. The first occurrence of noticeable solid-phase phosphatic material is in Sections 117-726A-2H, CC and 117-726A-3H, CC where yellow brown collophane replaces an assemblage of fish teeth and bones that resulted from thanatocoenosis. At the upper Pliocene unconformity ( $\sim 63$  mbsf) in Section 117-726A-7H, CC, we found a lag deposit of large (2 to 3 cm diameter) phosphorite nodules (carbonate fluorapatite) and pellets. These nodules and pellets exist throughout Cores 117-726A-8X, -9X and -10X (down to 92 mbsf). In the upper Miocene (Core 117-726A-11X), highly crystalline, transparent crystal aggregates of pure carbonate fluorapatite (francolite) were found within benthic foraminifer tests and as separate, coherent aggregates. These increase in abundance through Core 117-726A-14X ( $\sim 130$  mbsf). The general morphology, crystal form, and chemistry of the phosphorite at this site will require further study, but it is possible that phosphatization proceeds when sediment accumulation rates are low. However, organic matter diagenesis supplies sufficient phosphorus to the locus of mineralization (often the calcite substrate of foraminifers).

## ORGANIC GEOCHEMISTRY

### Abundance and Character of Organic Matter

Thirty-one samples of physical properties and headspace residues from Hole 726A were analyzed for organic carbon and carbonate content. The sample suite covers all lithologic units. Lithologic Unit I was subdivided into two subunits on lithological grounds (see "Lithostratigraphy" section, this chapter). Lithologic Subunit IA extends to approximately 32 mbsf and comprises bioturbated, nanofossil-rich, silty clay. Organic carbon concentrations are low and uniform (on average 0.67%; Table 2).

In contrast, lithologic Subunit IB (extending to 131.1 mbsf) shows elevated organic carbon concentrations in which hydrogen-rich organic matter predominates (high hydrogen index [HI] values; Figs. 33 and 34; Table 8). Subunit IB is similar in character to Subunit IA in the major lithology, except that it is less bioturbated and is composed of frequent lag deposits of silt- to sand-sized placers containing apatite, foraminifer tests, and other coarse-grained residues. These lag deposits seem disturbed by bioturbation. As suggested by the saw-tooth patterns in both the organic carbon concentration plot and the highly correlative HI, organic carbon in the bioturbated lag deposits and in the few centimeters of sediments on either side, is low (below 2%) and more refractory. In contrast, organic carbon concentrations in the interbedded, slightly bioturbated, hemipelagic silty clays reach values of up to 4.8% (Table 2), and the organic matter is characterized by high values.

The sole sample (117-726A-15X-1, 58–60 cm) analyzed of the dolomitic shallow-water limestones of Eocene age that comprise lithologic Unit II contained only 0.24% organic carbon. The calculated carbonate content of this sample is over 100%, a result of the fact that we are dealing with dolomite instead of carbonate. Smear slides of Cores 117-726A-13X and 117-726A-14X (see "Lithostratigraphy" section, this chapter) indicate a substantial amount of dolomite at the base of Subunit IA, and, therefore, the calculated carbonate values of these samples are too high. A sample of limestone from 141 mbsf has the lowest organic carbon value measured in Hole 726A.

Both the abundance and degree of preservation of sedimentary organic matter potentially reflect different oceanographic

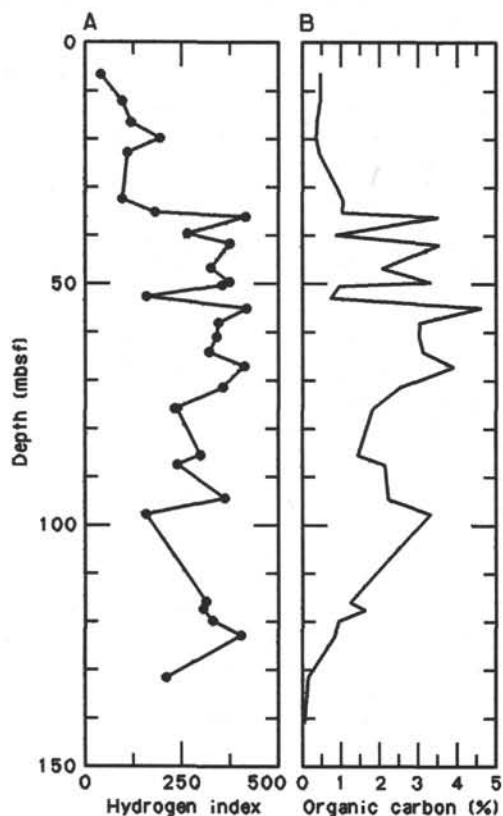


Figure 33. Downhole plot of organic carbon with hydrogen index values.

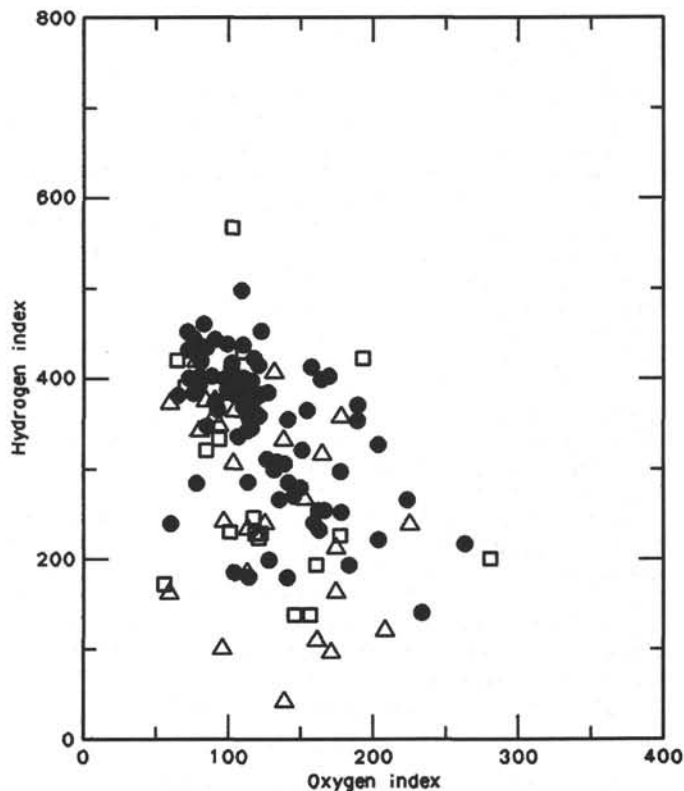


Figure 34. Plot of hydrogen index vs. oxygen index values of samples from sites within the oxygen-minimum zone on the Oman margin. Closed circles indicate samples from Site 723, triangles denote samples from Site 724, and squares depict samples from Site 726.

Table 8. Results of Rock-Eval pyrolysis of samples from Hole 726A.

Core, section, interval (cm)	Depth (mbsf)	T <sub>max</sub> (°C)	S <sub>1</sub>	S <sub>2</sub>	S <sub>3</sub>	S <sub>2</sub> /S <sub>3</sub>	TOC	HI	OI
117-726A-									
1H-5, 52-54	6.52	409	0.04	0.23	0.75	0.30	0.54	42	138
2H-4, 60-62	12.00	418	0.10	0.53	0.93	0.56	0.54	98	172
2H-7, 60-62	16.50	414	0.10	0.52	0.90	0.57	0.43	120	209
3H-3, 50-52	19.80	420	0.15	1.10	1.04	1.05	0.56	196	186
3H-5, 50-52	22.80	417	0.11	0.58	0.84	0.69	0.52	111	161
4H-5, 50-52	32.30	414	0.26	1.11	1.07	1.03	1.10	100	97
4H-7, 30-32	35.10	417	0.26	2.12	1.30	1.63	1.14	186	114
5H-1, 80-81	36.10	412	2.56	15.35	2.87	5.34	3.66	419	78
5H-3, 130-132	39.60	416	0.32	2.46	1.41	1.74	0.92	267	153
5H-5, 52-54	41.82	412	2.27	13.90	3.37	4.12	3.69	376	91
6H-2, 50-52	46.70	413	1.18	6.91	2.04	3.38	2.10	329	97
6H-4, 50-52	49.70	413	1.82	12.82	2.88	4.45	3.40	377	84
6H-4, 119-120	50.39	415	0.50	3.73	1.86	2.00	1.04	358	178
6H-6, 50-52	52.70	418	0.30	1.39	1.49	0.93	0.85	163	175
7X-1, 98-100	55.08	411	3.17	20.17	3.25	6.20	4.79	421	67
7X-3, 100-102	58.10	411	1.93	10.93	2.95	3.70	3.13	349	94
7X-5, 100-02	61.10	413	1.50	10.96	2.60	4.21	3.19	343	81
8X-1, 52-54	64.12	410	2.43	10.63	2.81	3.78	3.27	325	86
8X-3, 52-54	67.12	405	3.21	17.00	2.76	6.15	4.08	416	68
8X-6, 27-29	71.37	410	1.27	9.40	2.39	3.93	2.62	358	91
9X-2, 117-119	75.87	410	0.78	4.55	2.21	2.05	1.94	234	113
9X-2, 119-120	75.89	414	0.66	4.59	2.41	1.90	1.91	240	126
10X-2, 127-129	85.57	408	0.63	4.80	2.10	2.28	1.58	303	132
10X-4, 31-33	87.61	415	0.60	5.56	2.23	2.49	2.29	242	97
11X-2, 60-62	94.50	414	0.97	8.58	2.45	3.50	2.35	365	104
11X-4, 100-102	97.90	414	0.57	5.60	2.08	2.69	3.45	162	60
13X-3, 130-132	116.10	417	0.36	4.12	2.15	1.91	1.30	316	165
13X-4, 119-120	117.49	415	1.10	5.22	1.78	2.93	1.70	307	104
13X-6, 66-68	119.96	416	0.38	3.50	1.46	2.39	1.05	333	139
14X-2, 5-7	122.95	418	0.37	3.79	1.23	3.08	0.93	407	132

Note: HI = hydrogen index and OI = oxygen index. TOC values from coulometric determination. For a detailed description of parameters, refer to "Explanatory Notes" chapter (this volume).

conditions (e.g., high vs. low productivity) and/or different environmental conditions prevailing during deposition. The disparity between organic carbon concentrations and preservation between lithologic Subunits IA and IB, which seem quite similar in their inorganic sedimentary components, can be explained by either fluctuations in the primary productivity or in the position and oxygen content of the oxygen-minimum zone, or a combination of both. Presently, the upper boundary of the oxygen-minimum zone is near the water depth of Site 726 (331 m). The relative position of Site 726 may have migrated with respect to the zone, where the oxygen-depleted top of the oxygen-minimum zone impinges on the Oman margin. This scenario also implies that we consider benthic remineralization during oxic conditions to be more effective than when anoxia prevails in the water column because the lack of oxygen in bottom water inhibits bioturbation. Minimal or nonexistent bioturbation limits the rate at which oxidants (principally oxygen if bottom water is oxygenated, sulfate if it is anoxic) are delivered, either passively (through diffusion) or actively (through advection) to shallow buried sediments, thus enhancing preservation of organic matter. Visual examination of the cores suggests that bioturbation is limited in the organic-carbon-rich hemipelagic sequences of Subunit IB. These observations, coupled with the occasional occurrence of laminations and elevated HI values, seem to support the scenario described above. The apparent fluctuations of the oxygen-minimum zone might possibly have resulted directly from temporal variations during primary production.

#### Hydrocarbon Gases

A few measurements of interstitial hydrocarbon gas show consistently low methane concentrations, and no trace of thermogenic gas noted at other sites on the Oman margin (Table 9). The low values for biogenic methane imply that organic matter degradation during bacterial diagenesis in the entire sedimentary section is dominated by sulfate reduction.

### SUMMARY AND CONCLUSIONS

Site 726 marks the end point of a depth transect that brackets the depth range of a pronounced oxygen-minimum zone across the Oman continental margin. The site is located on what was assumed to be a pre-Neogene basement high that coincides with the shelf break, landward of a slope basin filled with thick (up to 2 km) Neogene sediment accumulations. The main objective at Site 726 was to identify the nature and age of rocks that underlie Neogene hemipelagic sediments covering much of the Leg 117 study area. Rapid vertical movements of the basement are evident in seismic images and provided the subsidence necessary for the immense sedimentation rates found in slope basins off Oman. Another reason for drilling at Site 726 was to investigate the facies of sediments at the present upper boundary of this oxygen-minimum zone and to examine the record for changes in the position of the oxygen-minimum zone in the Neogene.

**Table 9. Results of headspace analysis for interstitial gas at Site 726.**

Core, section, interval (cm)	Depth (mbsf)	C <sub>1</sub> (μL/L)
117-726A-		
3H-4, 119-120	21.99	32
6H-4, 119-120	50.39	35
9X-2, 119-20	75.89	54
13X-4, 119-120	117.49	19

The main findings at Site 726 are summarized in Figure 35 and include the identification of:

1. The recovery of shallow-water limestones of Eocene age (?) similar to those that unconformably overlie the ophiolitic basement on the island of Masirah to the north.
2. The discovery of a hiatus that spans at least 30 m.y. between the Eocene (?) shallow-water limestones and the hemipelagic sediment cover of late Miocene to Holocene age.
3. Indications of repeated alternations of anoxic conditions that result in laminated layers (which are also organic-rich) with conditions of winnowing and oxygenation that result in bioturbated lag deposits.
4. The preservation of biogenic opal in the upper Pliocene that parallels opal preservation at other sites on the margin.
5. A possible water source with high chlorinity in or overlying the Eocene (?) limestones.

The section at Site 726 was divided into two lithologic units that are separated by a pronounced hiatus spanning the time from the late Miocene to the Eocene. The lithologic character of these units differs considerably (Fig. 35).

Unit I (0-131.1 mbsf) is subdivided into two subunits. Subunit IA comprises bioturbated, phosphorite-bearing, nannofossil-rich, calcitic, silty clay to clayey silt—sediments similar to those found at other sites that are typical for the deposits underlying highly productive upwelling cells. The mean sedimentation rate for Subunit IA (NN21 to NN19) is approximately 45 m/m.y. (Fig. 35). Subunit IB is similar in composition to Subunit IA, but is characterized by laminated intervals in its upper half and by frequent lag deposits throughout the subunit (Fig. 35). These lag deposits contain sand-sized foraminifers, phosphoritic grains, fish teeth, and bones that are intercalated in the hemipelagic sequence. These deposits are considered indicators of current winnowing. The frequency of these lag deposits decreases upsection, which indicate progressive deepening of the site. This inference is supported by the increase of the planktonic-benthic ratio upsection. In accordance with recurrent winnowing or non-deposition, the section of Subunit IB is greatly compressed and has an average sedimentation rate of about 15 m/m.y. (Fig. 35).

Lithologic Unit II was only sparsely recovered from 131.1 to 186.3 mbsf and consists of nummulitic and oncolitic limestone of Eocene (?) age, which was variably cemented by dolomite and calcite. These shallow-water sediments appear to correspond to limestone occurrences described from the Arabian peninsula and the ophiolite complex of Masirah, where similar sediments unconformably overlie ophiolitic basement. The base of this recovered section may be slightly silicified.

Paleontological investigation revealed two major hiatuses. The first separates Pleistocene from upper Pliocene hemipelagic sediments, while the second corresponds to the transition from Eocene (?) limestone to upper Miocene transgressive biogenic and eolian upwelling deposits (Fig. 35). The hiatus between upper Pliocene and Pleistocene truncates an interval where radiolarians and diatoms indicate influence of colder water or water of different nutrient composition at the site. This interval seems coeval with similar occurrences at the deeper water Sites 723 and 724, where an opal-rich interval was expanded.

Laminated deposits occur in the upper Pliocene and the lower Pleistocene section (Fig. 35). The upper Pliocene laminations coincide with the opal-rich zone and alternate with lag deposits, while only about one-half of the lower Pleistocene laminations are associated with lag deposits. This interval of laminated deposits spans a large range of accumulation rates and possibly several hiatuses. The association of laminated sequences, lag

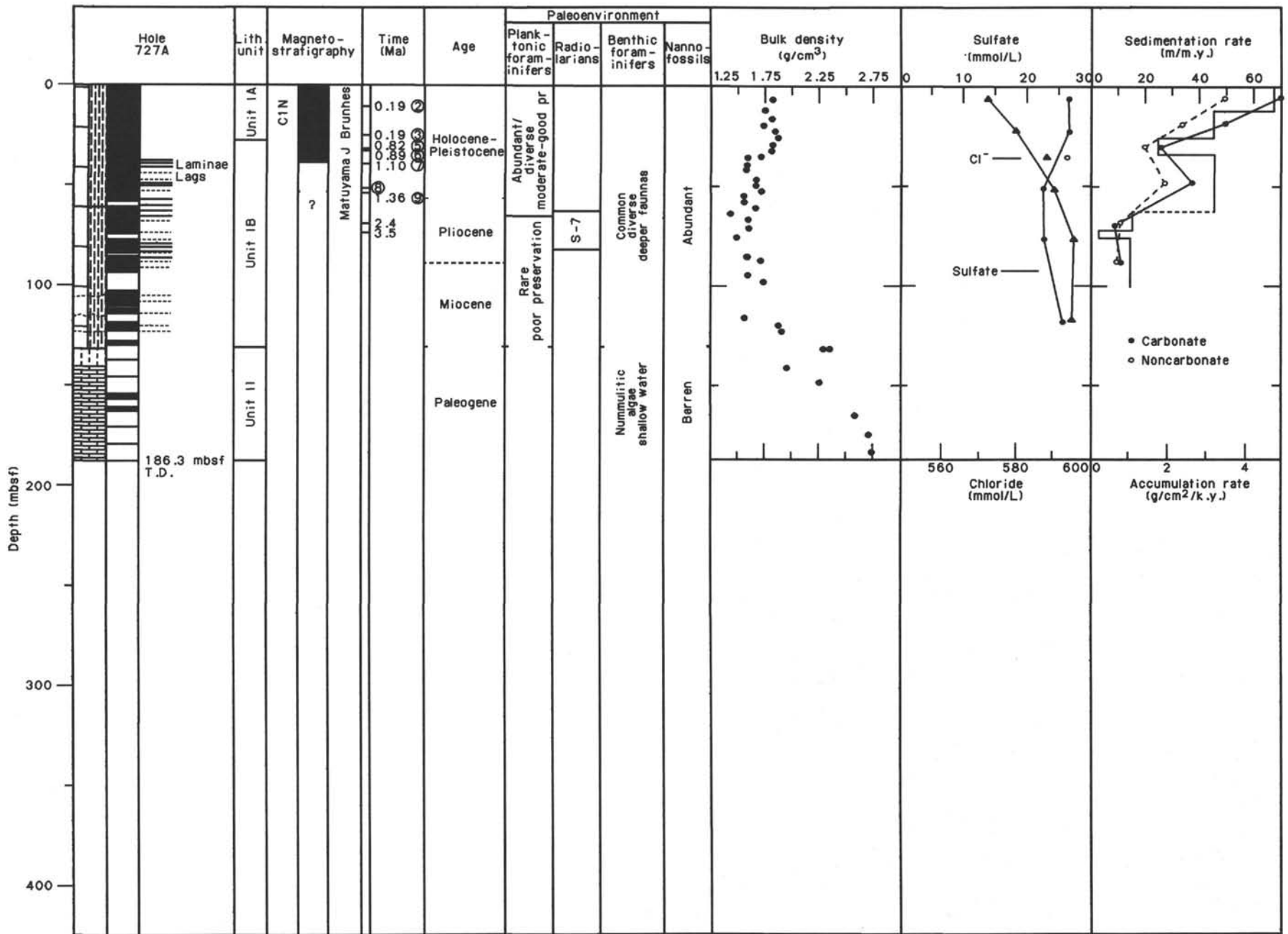


Figure 35. Summary chart outlining preliminary shipboard findings at Site 726.

deposits, and variations in bioturbation indicate variations in the intensity of the oxygen-minimum zone and of current winnowing, possibly by the upwelling countercurrent.

Poor recovery in the variably indurated and lithified limestone and dolostone precluded continuously sampling interstitial water and impeded sampling for interstitial gas. However, a high chloride concentration of 600 mmol/L suggests that hypersaline water either is present in the subsurface or is advected horizontally to the site (Fig. 35). Chemical data also show that Site 726 has more phosphate and less silica than other sites on the margin.

Sediments recovered at Site 726 did not yield the nature or age of the igneous basement complex that underlies this area of the Oman margin. However, by comparison with sediments overlying ophiolitic basement on the island of Masirah, we believe that the shallow-water limestone sequence recovered here and at Site 729 may be associated with ophiolitic basement. The occurrence of the shallow-water, biogenic, carbonate sediments implies that the Oman margin may have been a starved carbonate platform before possible subaerial exposure and erosion near the wave base during much of the Paleogene and early Neogene. We believe that the hemipelagic sediments deposited since the late Miocene on top of the shallow-water carbonates record a progressive deepening of the environment, because placerlike lag deposits are less frequent and the planktonic-benthic ratio increases upsection. The environment alternated between states conducive to the formation of lamination and preservation of labile organic matter and those conducive to bioturbation and current winnowing. Evidence linking the oscillations to either eustatic sea level, vertical tectonic movements, or variations in the oxygen-minimum zone are inconclusive and will be the focus of post-cruise research.

## REFERENCES

- Bathurst, R.G.C., 1975. *Carbonate Sediments and Their Diagenesis*. Developments in Sedimentology (Vol. 12): New York-London-Amsterdam (Elsevier).
- Baturin, G. N., 1971. Formation of phosphate sediments and water dynamics. *Oceanology*, 11:372-376.
- Berggren, W. A., Kent, D. V., and Van Couvering, J. A., 1985. The Neogene: Part 2, Neogene geochronology and chronostratigraphy. In Snelling, N. J. (Ed.), *The Chronology of the Geological Record*. Geol. Soc. Mem. (London), 10:211-259.
- Burnett, W. C., 1977. Geochemistry and origin of phosphorite deposits from off Peru and Chile. *Geol. Soc. Am. Bull.*, 88:813-823.
- Clement, B. M., and Robinson, F., 1987. The magnetostratigraphy of Leg 94 sediments. In Ruddiman, W. F., Kidd, R. B., Thomas, E., et al., *Init. Repts. DSDP*, 94, Pt. 2: Washington (U.S. Govt. Printing Office), 635-650.
- Haq, B. U., Hardenbol, J., and Vail, P. R., 1987. Chronology of fluctuating sea levels since the Triassic. *Science*, 235:1156-1167.
- Moseley, F., and Abbotts, I. L., 1979. The ophiolite melange of Masirah, Oman. *J. Geol. Soc. London*, 136:713-724.
- Powers, R. W., Ramirez, L. F., Redmond, C. D., and Elberg, E. L., 1966. Geology of the Arabian peninsula: sedimentary geology of Saudi Arabia. *U.S. Geol. Surv. Prof. Pap.*, 560D.
- Sato, T., Takayama, T., Kato, M., Kudo, T., and Kamei, K., in press. Calcareous microfossil biostratigraphy of the uppermost Cenozoic formations distributed in the coast of the Japan Sea. Part 4: Conclusion. *Sekiyu Gijutsu Kyokaishi*.
- Takayama, T., and Sato, T., 1987. Coccolith biostratigraphy of the North Atlantic Ocean, Deep Sea Drilling Project Leg 94. In Ruddiman, W. F., Kidd, R. B., Thomas, E., et al., *Init. Repts. DSDP*, 94, Pt. 2: Washington (U.S. Govt. Printing Office), 651-702.

Ms 117A-113